Mantoniella beaufortii and Mantoniella baffinensis sp. nov. (Mamiellales, Mamiellophyceae), two new green algal species from the high arctic

Sheree Yau, Adriana Lopes dos Santos, Wenche Eikrem, Catherine Gérikas Ribeiro, Priscillia Gourvil, Sergio Balzano, Marie-line Escande, Hervé Moreau, Daniel Vaulot

MANTONIELLA BEAUFORTII AND *MANTONIELLA BAFFINENSIS* SP. NOV. (MAMIELLALES, MAMIELLOPHYCEAE), TWO NEW GREEN ALGAL SPECIES FROM THE HIGH ARCTIC[1]

Sheree Yau[2,3]

Integrative Marine Biology Laboratory (BIOM), CNRS, UMR7232, Sorbonne Université, Banyuls sur Mer, France.

Adriana Lopes dos Santos

Asian School of the Environment, Nanyang Technological University, 50 Nanyang Avenue, Singapore

Centro de Genómica, Ecología y Medio Ambiente, Facultad de Ciencias, Universidad Mayor. Camino La Pirámide 5750, Huechuraba. Santiago, Chile.

Wenche Eikrem

Norwegian Institute for Water Research, Gaustadallèen 21, 0349, Oslo, Norway.

University of Oslo, Department of Biosciences, P.O. box 1066 Blindern, 0316, Oslo, Norway.

Natural History Museum, University of Oslo, P.O. box 1172 Blindern, 0318 Oslo, Norway.

Catherine Gérikas Ribeiro and Priscillia Gourvil

Sorbonne Université, CNRS, UMR7144, Station Biologique de Roscoff, Roscoff, France.

Sergio Balzano

Stazione Zoologica Anton Dohrn, Istituto Nazionale di Biologia, Ecologia e Biotecnologie Marine, Naples, Italy.

Marie-Line Escande and Hervé Moreau

Integrative Marine Biology Laboratory (BIOM), CNRS, UMR7232, Sorbonne Université, Banyuls sur Mer, France.

Daniel Vaulot

Sorbonne Université, CNRS, UMR7144, Station Biologique de Roscoff, Roscoff, France.

Asian School of the Environment, Nanyang Technological University, 50 Nanyang Avenue, Singapore.

[2]Corresponding author: Sheree Yau, sheeyau@gmail.com

[3]Present address: Department of Marine Biology and Oceanography, Institute of Marine Sciences (ICM), CSIC, Barcelona, Spain.

Running Title: *Mantoniella* species from the high Arctic

Abstract

Members of the class Mamiellophyceae comprise species that can dominate picophytoplankton diversity in polar waters. Yet polar species are often morphologically indistinguishable from temperate species, although clearly separated by molecular features. Here we examine four Mamiellophyceae strains from the Canadian Arctic. The 18S rRNA and Internal Transcribed Spacer 2 (ITS2) gene phylogeny place these strains within the family Mamiellaceae (Mamiellales, Mamiellophyceae) in two separate clades of the genus *Mantoniella*. ITS2 synapomorphies support their placement as two new species, *Mantoniella beaufortii* and *Mantoniella baffinensis*. Both species have round green cells with diameter between 3–5 µm, one long flagellum and a short flagellum (~1 µm) and are covered by spiderweb-like scales, making both species similar to other *Mantoniella* species. Morphologically, *M. beaufortii* and *M. baffinensis* are most similar to the cosmopolitan *M. squamata* with only minor differences in scale structure distinguishing them. Screening of global marine metabarcoding datasets indicates *M. beaufortii* has only been recorded in seawater and sea ice samples from the Arctic while no environmental barcode matches *M. baffinensis*. Like other Mamiellophyceae genera that have distinct polar and temperate species, the polar distribution of these new species suggests they are cold or ice-adapted *Mantoniella* species.

Key index words: Arctic; ITS; Mamiellophyceae; *Mantoniella*; metabarcoding; picophytoplankton; polar

Abbreviations: rRNA, ribosomal RNA; ITS2, internal transcribed spacer 2; compensatory base change, CBC; hemi-CBC, hCBC; TEM, transmission electron microscopy

Introduction

Over the last decades the taxonomy of the green algae has gone through a profound reorganization. The class Prasinophyceae, initially defined as scaly flagellates (Moestrup and Throndsen 1988), has been rearranged into several new classes such as the Chlorodendrophyceae, Chloropicophyceae and Mamiellophyceae (Massjuk 2006, Marin and Melkonian 2010, Lopes dos Santos et al. 2017b) as well as clades without formal names (Guillou et al. 2004, Tragin et al. 2016) leading to the class name Prasinophyceae to be abandoned. The Mamiellophyceae are ecologically successful and particularly dominant in marine coastal waters (Lopes dos Santos et al. 2017a, Tragin and Vaulot 2018). The first scaled species of Mamiellophyceae observed were *Mantoniella squamata* (as *Micromonas squamata*, Manton and Parke 1960) and *Mamiella gilva* (as *Nephroselmis gilva*, Parke and Rayns 1964). Moestrup (1984) erected the family Mamiellaceae, which included *Mantoniella* and *Mamiella,* with *Mamiella gilva* designated as the type species. Mamiellophyceae comprises three orders: Monomastigales, with one freshwater genus *Monomastix*; Dolichomastigales, with two genera *Crustomastix* and *Dolichomastix*; Mamiellales, which currently comprises five genera *Bathycoccus*, *Mamiella*, *Mantoniella*, *Micromonas* and *Ostreococcus.* As these genera are morphologically heterogeneous, with *Micromonas* and *Ostreococcus* lacking scales and *Bathycoccus* and *Ostreococcus* lacking flagella, the monophyly of Mamiellophyceae was established based on nuclear and plastid rRNA sequence and secondary structure analyses (Marin and Melkonian 2010).

Molecular analyses of the Mamiellophyceae have permitted the description of otherwise morphologically indistinguishable cryptic species. For example, wide genetic diversity has been shown to exist between morphologically identical *Ostreococcus* species where less than 1%

difference in the 18S rRNA gene corresponds to up to 30% of variation in orthologous protein coding sequences (Palenik et al. 2007, Piganeau et al. 2011). From an early stage, 18S rRNA-defined clades of *Micromonas* and *Ostreococcus* were observed to have distinct geographic distributions, suggesting their genetic variation reflected adaptations to ecological niches (Rodríguez et al. 2005, Foulon et al. 2008) and that these clades represented distinct species. *Ostreococcus* is divided into rare species restricted to estuarine (*O. mediterraneus*) and coastal environments (*O. tauri*), as well as more abundant oceanic species (*O. lucimarinus* and clade B) (Demir-Hilton et al. 2011, Treusch et al. 2012, Hu et al. 2016, Simmons et al. 2016). *Micromonas* cells were observed to be abundant in the Arctic Ocean (Throndsen and Kristiansen 1991, Sherr et al. 2003, Not et al. 2005) that subsequent 18S rRNA analyses revealed them to belong to a clade with an Arctic distribution (Lovejoy et al. 2007, Balzano et al. 2012). *Micromonas* has since been revised defining the Arctic clade as the species *M. polaris*, and species originating from lower latitudes as *M. bravo*, *M. commoda* and *M. pusilla* (Simon et al. 2017). Similarly, in *Mantoniella*, *M. antarctica* was described from the Antarctic whereas *M. squamata* was cosmopolitan (Marchant et al. 1989).

Three picophytoplanktonic strains (RCC2285, RCC2288 and RCC2497) were isolated in the Canadian Arctic from mesophilic surface water sampled at two sites in the Beaufort Sea in the summer of 2009 as part of the MALINA cruise (Balzano et al. 2012). A fourth strain (RCC5418) was subsequently isolated from sea ice collected in Baffin Bay in the spring as part of the Green Edge project. We performed a combination of molecular, morphological and pigment characterization of these isolates, which we propose to constitute two novel *Mantoniella* species, *M. beaufortii* and *M. baffinensis*, restricted to polar environments.

Methods

Culture conditions. Strains RCC2285, RCC2288, and RCC2497 were isolated from seawater collected at two sites (70°30'N, 135°30'W and 70°34'N, 145°24W) in the Beaufort Sea in the summer of 2009 as part of the MALINA cruise as described previously (Balzano et al. 2012). Strain RCC5418 was isolated from the Green Edge project Ice Camp (http://www.greenedgeproject.info/), a sampling site on the sea ice near the village of Qikiqtarjuaq (67°28.784N, 63°47.372W). Sampling was conducted between 20 April and 27 July, 2016, beginning in completely snow covered conditions followed by bare ice and ending when the ice was broken out. Sea ice from 23 May 2016 was melted overnight and 200 mL was gravity filtered (Sartorius filtration system) through 3 µm pore size polycarbonate filters (Millipore Isopore membrane, 47 mm). 500 µL of filtrate was enriched by addition to 15 mL of L1 medium (NCMA, Bigelow Laboratory for Ocean Sciences, USA). The enrichment culture was purified by dilution to 10 cells per well in a 96 deep-well plate (Eppendorf) and incubated under white light (100 µE m^{-2} s^{-1}) in a 12:12 h light: dark cycle at 4°C. Cell growth was observed by the development of coloration after a few weeks. Culture purity was assessed by flow cytometry (Becton Dickinson, Accuri C6). After confirmation of the purity, the culture was transferred in a 50 mL ventilated flask (Sarstedt). Cultures are maintained in the Roscoff Culture Collection (http://roscoff-culture-collection.org/) in K/2 (Keller et al. 1987) or L1 medium at 4ºC under a 12:12 h light: dark cycle at 100 µE light intensity. RCC2285 has been lost from culture since molecular analyses (described below) were performed. For pigment analysis and electron microscopy, RCC2288 was grown at 7ºC under continuous light at 100 µE intensity in L1 medium prepared using autoclaved seawater from offshore Mediterranean Sea water diluted 10% with MilliQ water and filtered prior to use through 0.22 µm filters. Holotype specimens

were deposited in O (Natural History Museum, University of Oslo), herbarium acronym follows Thiers (2019).

Sequences. Nuclear 18S rRNA and the Internal Transcribed Spacers (ITS) 1 and 2, as well as the 5.8S rRNA gene were retrieved from GenBank for strains RCC2288, RCC2497 and RCC2285 (Balzano et al. 2012). For RCC5418 and RCC5150 (*M. antarctica*), cells were harvested in exponential growth phase and concentrated by centrifugation. Total nucleic acids were extracted using the Nucleospin Plant II kit (Macherey-Nagel, Düren, DE) following the manufacturer's instructions. The nearly full length nuclear 18S rRNA gene (only RCC5418) and the region containing the Internal Transcribed Spacers (ITS) 1 and 2, as well as the 5.8S rRNA gene were obtained by PCR amplification using universal primers (Supplementary Table 1). PCR products were directly sequenced at the Macrogen Company (Korea) and sequences have been deposited to Genbank under accession numbers MH516003, MH516002 and MH542162.

ITS2 secondary structure. The ITS2 secondary structure from the strains listed in Table 1 was predicted using the Mfold web interface (Zuker 2003) under the default options with the folding temperature fixed at 37ºC, resulting in multiple alternative folding patterns per sequence. The preliminary structure for each sequence was chosen based on similarities found among the other structures proposed for Mamiellophyceae (Marin and Melkonian 2010, Simon et al. 2017) as well as on the presence of previously defined ITS2 hallmarks defined by Coleman (Mai and Coleman 1997, Coleman 2000, 2003, 2007). Exported secondary structures in Vienna format and the respective nucleotide sequences were aligned, visualized using 4SALE version 1.7 (Seibel et al. 2008) and manually edited through extensive comparative analysis of each position

148 (nucleotide) in sequences from representatives of the Mamiellophyceae. The ITS2
149 synapomorphy analysis was confined to those positions that formed conserved base pairs in all
150 members of the Mamiellaceae order and the resulting intramolecular folding pattern (secondary
151 structure) of *Mantoniella* was drawn using CorelDRAW X7. A Vienna file containing the ITS2
152 sequences and secondary structure is available at
153 https://doi.org/10.6084/m9.figshare.7472153.v1.
154
155 *Phylogenetic analyses*. Nuclear 18S rRNA sequences belonging to members of
156 Mamiellophyceae were retrieved from GenBank (http://www.ncbi.nlm.nih.gov/). Two
157 environmental sequences (similar to strain sequences) were included in addition to the sequences
158 obtained from the cultures. Sequences were also obtained for the ITS2 region located between
159 the 5S and 23S rRNA genes. However, no environmental sequences were available to be
160 included in the 18S/ITS phylogenetic analyses.
161 Twenty-seven nuclear 18S rRNA and fourteen ITS2 sequences were aligned with MAFFT
162 using the E-INS-i and G-INS-i algorithms respectively (Katoh and Toh 2008). Alignments were
163 visualized and manually edited using Geneious 10.2.5 (Kearse et al. 2012). The ITS2 alignment
164 was further edited on the basis of conserved secondary structures (see above). The nuclear 18S
165 rRNA and ITS2 sequences from the Mamiellaceae members were concatenated using Geneious
166 10.2.5 (Kearse et al. 2012). Lengths of the resulting alignments were 1567 bp for 18S rRNA
167 (1242 identical sites, 295 variable and 191 parsimony-informative sites) and 1875 bp for
168 concatenated 18S-ITS sequences (1544 identical sites, 302 variable and 179 parsimony-
169 informative).

Phylogenetic reconstructions with two different methods, maximum likelihood (ML) and Bayesian analyses, were performed using the nuclear Mamiellophyceae 18S rRNA and Mamiellaceae concatenated 18S/ITS2 alignments.

The K2 + G + I model was selected for both sequence datasets based on the substitution model selected through the Akaike information criterion (AIC) and the Bayesian information criterion (BIC) options implemented in MEGA 6.06 (Tamura et al. 2013). ML analysis was performed using PhyML 3.0 (Guindon et al. 2010) with SPR (Subtree Pruning and Regrafting) tree topology search operations and approximate likelihood ratio test with Shimodaira-Hasegawa-like procedure. Markov chain Monte Carlo iterations were conducted for 1,000,000 generations sampling every 100 generations with burning length 100,000 using MrBayes 3.2.2 (Ronquist and Huelsenbeck 2003) as implemented in Geneious (Kearse et al. 2012). Nodes were considered as well supported when SH-like support values and Bayesian posterior probabilities were higher than 0.8 and 0.95 respectively. The same criteria were used to represent the sequences on the phylogenetic trees. Alignments are available at https://doi.org/10.6084/m9.figshare.7472153.v1.

Screening of environmental 18S rRNA sequencing datasets. High-throughput sequencing metabarcodes (V4 and V9 hypervariable regions) were obtained from several published polar studies, as well as from the global sampling efforts Tara Oceans and Ocean Sampling Day (OSD) (see Supplementary Table 2 for the full details and references for each project). We screened these data as well as GenBank by BLASTn (98% identity cut-off) using RCC2288 18S rRNA gene sequence as the search query. We aligned the retrieved environmental sequences and metabarcodes with that of RCC2285, RCC2288, RCC2497, and RCC5418 using MAFFT as implemented in Geneious version 10.0.7 (Kearse et al. 2012). This allowed the determination of

sequence signatures diagnostic of this species for both V4 and V9 (Supplementary Figures 1 and 2). The oceanic distribution of stations where cultures, clones and metabarcodes having these signatures, as well as the stations from the metabarcoding surveys where no matching metabarcodes have been found, were plotted with the R libraries ggplot2 and rworldmap. The R script is available at https://vaulot.github.io/papers/RCC2288.html.

Light microscopy. Cells were observed using an Olympus BX51 microscope (Olympus, Hamburg, Germany) with a 100× objective using differential interference contrast (DIC) and imaged with a SPOT RT-slider digital camera (Diagnostics Instruments, Sterling Heights, MI, USA).

For video-microscopy, cultures from RCC2288 and RCC2497 were observed with an inverted Olympus IX70 inverted microscope using an x40 objective and equipped with an Infinity X camera (https://www.lumenera.com/products/microscopy/infinityx-32.html). Short sequences were recorded and edited with the Video de Luxe software (http://www.magix.com/fr/video-deluxe/). Films were uploaded to Youtube (https://www.youtube.com/channel/UCsYoz-aSJlJesyDNj6ZVolQ/videos). Video microscopy of swimming behavior of RCC2288 (https://youtu.be/CGKNxzfGUvQ), RCC2497 (https://youtu.be/rRNuk5Lx7Aw), and RCC5418 (https://youtu.be/xoxCEl1cv4Q). The recording protocol is available at dx.doi.org/10.17504/protocols.io.k24cygw.

Transmission Electron Microscopy. Positive-stained whole mount cells were prepared as described by Moestrup (1984), where cultures were directly deposited on formvar coated copper grids and stained with 2% uranyl acetate. TEM thin-sections was performed as previously

described (Derelle et al. 2008). Briefly, fixed RCC2288 cells (1% glutaraldehyde) from an exponentially growing culture were suspended in molten (37°C) 1% low melting point agarose. The agarose cell plug was fixed, washed, dehydrated in ethanol and embedded in Epon 812. Ultra-thin sections (80–90 nm) were placed on a 300 mesh copper grid and stained with uranyl acetate for 15 min, followed by lead citrate staining for 2 min. The cells were visualized with Hitachi H 7500 and H-9500 transmission electron microscopes.

Pigment analysis. Pigments were extracted from RCC2288 cells in late exponential phase as previously described (Ras et al. 2008). Briefly, cells were collected on 0.7 µm particle retention size filters (GF/F Whatman), pigments extracted for 2 hours in 100% methanol, then subjected to ultrasonic disruption and clarified by filtration through 0.2 µm pore-size filters (PTFE). Pigments were detected using high performance liquid chromatography (HPLC, Agilent Technologies 1200) over the 24 h after the extraction.

Results and Discussion

Taxonomy section. Mantoniella beaufortii Yau, Lopes dos Santos and Eikrem sp. nov.

Description: Cells round measuring 3.7 ± 0.4 µm in diameter with one long (16.3 ± 2.6 µm) and one short flagellum (~1 µm). Cell body and flagella covered in imbricated spiderweb scales. Flagellar hair scales present composed of two parallel rows of subunits. Long flagellum tip has tuft of three hair scales. Scales produced in Golgi body. Golgi body located beneath and to one side of basal bodies. One green chloroplast with pyrenoid surrounded by starch and a stigma composed of a single layer of oil droplets (~0.1 µm). Ejectosomes composed of fibrils located at periphery of cell. Cell bodies with sub-quadrangular to oval scales (~0.2 µm). Body scales

heptaradial, with seven major spokes radiating from center, number of spokes increasing towards the periphery. Six or more concentric ribs divide the scale into segments. Flagella with hexaradial oval scales composed of six spokes increasing in number towards the periphery. Six or more concentric ribs divide the scale into segments. Combined nucleotide sequences of the 18S rRNA (JN934679) and ITS2 rRNA (JQ413369) are species specific.

Holotype: Accession number O-A10010, plastic embedded specimen, 14 July 2009, from surface water, MALINA cruise leg 1b. Figure 4 shows cells from the embedding. Culture deposited in The Roscoff Culture Collection as RCC2288.

Type locality: Beaufort Sea in the Arctic Ocean (70°30'N, 135°30'W).

Etymology: Named for its geographical provenance.

Mantoniella baffinensis Yau, Lopes dos Santos and Eikrem sp. nov.

Description: Cells measuring 4.7 ± 0.5 μm with one long flagellum of 21.8 ± 5.1 μm and one short flagellum (~1 μm). Cell body and flagella covered in imbricated spiderweb scales. Flagellar hair scales present composed of two parallel rows of subunits. Long flagellum tip has tuft of three hair scales. Cell bodies with sub-quadrangular to oval scales (~0.2 μm). Body scales octaradial with eight major radial spokes radiating from center, number of spokes increasing towards the periphery. Seven or more concentric ribs divide the scale into segments. Flagella with heptaradial, oval scales composed of seven spokes increasing in number towards the periphery. Six or more concentric ribs divide the scale into segments. Combined nucleotide sequences of the nuclear 18S rRNA (MH516003) and ITS2 rRNA (MH542162) are species specific.

Holotype: Accession number O-A10011, plastic embedded specimen, 23 May 2016, from surface sea ice, Green Edge project Ice Camp. Culture deposited in The Roscoff Culture Collection as RCC5418.

Type locality: Surface sea ice off the coast of Baffin Island in Baffin Bay (67°28'N, 63°46'W).

Etymology: Named for its geographical provenance.

Phylogeny and ITS signatures. The phylogenetic tree based on nearly full-length nuclear 18S rRNA sequences obtained from the novel polar strains RCC2288, RCC2285, RCC2497 and RCC5418 (Table 1), and environmental sequences retrieved from GenBank indicated that these strains belong to the family Mamiellaceae (Supplementary Figure 3). The analysis also recovered the major genera within Mamiellales: *Bathycoccus*, *Ostreococcus*, *Micromonas*, *Mantoniella* and *Mamiella* (Marin and Melkonian 2010). Dolichomastigales and Monomastigales were the basal orders in Mamiellophyceae with *Monomastix opisthostigma* type species used as an outgroup. Strains RCC2485, RCC2288 and RCC2497 isolated during the MALINA cruise in the Beaufort Sea and strain RCC5418 isolated from Baffin Bay during the Green Edge project Ice Camp formed a well-supported clade together with two environmental sequences (clone MALINA St320 3m Nano ES069 D8 and clone 4-E5), which also originated from Arctic Ocean samples. The two described *Mantoniella* species (*M. squamata* and *M. antarctica*) were not monophyletic in our analysis using the nuclear 18S rRNA, as reported by Marin and Melkonian (2010) (Supplementary Figure 3).

In contrast, the phylogenetic tree based on concatenated 18S/ITS2 alignments suggested that our strains belong in *Mantoniella* (Figure 1). The grouping of our strains within *Mantionella* in the concatenated 18S/ITS tree was consistent with a recent nuclear multigene phylogeny based

283 on 127 concatenated genes from related Chlorophyta species that also included RCC2288 with
284 *Mantoniella* species (Lopes dos Santos et al. 2017b). This indicated the 18S/ITS2 tree reflects
285 the evolutionary history of the nuclear genome supporting the position of *Mantoniella* and our
286 strains diverging from the same common ancestor.
287 The average distance between strains RCC2485, RCC2288 and RCC2497 was low (0.5% of
288 segregating sites over the near full-length 18S rRNA gene), suggesting that these strains
289 corresponded to a single species that we named *Mantoniella beaufortii* (see Taxonomy section).
290 In contrast, the well-supported placement of strain RCC5418 on an earlier diverging branch
291 within the *Mantoniella* clade, as well as the 1% average distance between RCC5418 and the
292 other strains, suggested it represents another species, named here *Mantoniella baffinensis*.
293 To substantiate the description of *M. beaufortii* and *M. baffinensis* as new species, we
294 investigated ITS2 synapomorphies of the different *Mantoniella* species. Although the use of
295 ITS2 in taxonomy should be considered with caution (Müller et al. 2007, Caisová et al. 2011),
296 several studies have shown the power of using ITS2 sequences in delimiting biological species,
297 especially in microalgal studies (e.g. Coleman 2007, Caisová et al. 2011) including green algae
298 (Subirana et al. 2013, Simon et al. 2017). For example, ITS sequencing contributed to
299 distinguishing the Arctic diatom *Chaetoceros neogracilis* from an Antarctic *Chaetoceros* sp. that
300 shared nearly identical 18S rRNA genes (Balzano et al. 2017). The analysis of ITS2 secondary
301 structure in addition to molecular signatures of nuclear and plastid SSU rRNA genes supported
302 the description of Chloropicophyceae clades as distinct species, despite the absence of clear
303 morphological differences (Lopes dos Santos et al. 2017b). This conclusion has been further
304 supported by recent phylogenetic analyses of chloroplast and mitochondrial genomes (Turmel et
305 al. 2019). The computed ITS2 secondary structure of the new *Mantoniella* strains contained the

four helix domains found in many eukaryotic taxa (Supplementary Figure 4), in addition to Helix B9. The intramolecular folding pattern of the ITS2 transcript from *M. beaufortii* and *M. baffinensis* was very similar to the one from *M. squamata* and *M. antarctica* (Supplementary Figure 4). The universal hallmarks proposed by Mai and Coleman et al. (1997) and Schultz et al. (2005) were present in Helices II and III of the Mamiellaceae. These were the Y-Y (pyrimidine-pyrimidine) mismatch at conserved base pair 7 in Helix II (Figure 2) and YRRY (pyrimidine-purine-pyrimidine) motif at conserved positions 28–31 on the 5' side of Helix III (Supplementary Figure 5A). In all four strains, the Y-Y mismatch was represented by the pair U-U and the YRRY motif by the sequence UGGU.

The structural comparison at each base pair position within the ITS2 helices identified several compensatory base changes (CBCs) and single-side changes or hemi-CBCs (hCBCs), as well as conserved base pair positions among *Mantoniella* species (Supplementary Figure 4). Note that we only considered hCBCs at positions where the nucleotide bond was preserved. No CBCs were found between the three *M. beaufortii* strains consistent with their designation as a single species. However, three hCBCs were detected in Helix II at positions 15 and 17 (Figure 2) and Helix III at position 12 (Supplementary Figure 5A). Three CBCs were detected in Helices I (position 4), II (position 15) and IV (position 22) between *M. beaufortii* and *M. baffinensis*, supporting the separation of these strains into two distinct species (Figure 2 and Supplementary Figure 4). When possible, the evolutionary steps of the identified CBCs and hCBCs were mapped upon branches of the Mamiellaceae phylogenetic tree that was constructed based on the concatenated 18S/ITS2 (Figure 2 and Supplementary Figure 4) to distinguish synapomorphies from homoplasious changes (e.g. parallelisms and reversals). Few hypervariable positions showing several changes (CBCs and hCBCs) could not be unambiguously mapped upon the tree.

329

330 *Morphology and ultrastructure.* Under light microscopy, the cells of the new strains were green
331 and round with one long and one short reduced flagellum (~1 μm), which were inserted almost
332 perpendicularly to the cell (Figure 3). They swam with their flagella directed posteriorly, pushing
333 the cell. Occasionally the cells ceased movement, pirouetted and took off again in a different
334 direction (video links in the Materials and Methods). All strains possessed a stigma, visible in
335 light microscopy as a red eyespot located opposite the flagella. Although there are no
336 morphological characters that are unique to the mamiellophyceans and shared by all of its
337 members, the new strains closely resembled *Mantoniella* and *Mamiella*, which are similarly
338 small round bi-flagellated cells (see Supplementary Table 3 for morphological characters in
339 described Mamiellophyceae). However, the flagella of *Mamiella* are of equal or near equal
340 lengths (Moestrup 1984), so clearly the unequal flagella observed in our strains conform with
341 described *Mantoniella* species, *M. squamata* and *M. antarctica* (Barlow and Cattolico 1980,
342 Marchant et al. 1989). The new strains were thus morphologically indistinguishable by light
343 microscopy from *Mantoniella* species, supporting their placement in the genus.
344 The new strains were in the size range (Table 2) reported for *M. squamata* (3–6.5 μm) and
345 *M. antarctica* (2.8–5 μm) (Manton and Parke 1960, Marchant et al. 1989). Nonetheless,
346 *M. beaufortii* strains were significantly smaller than *M. baffinensis* in cell diameter and average
347 long flagellum length (Table 2) providing a means to distinguish the two new *Mantoniella*
348 species from each other with light microscopy.
349 Transmission Electron Microscopy (TEM) of thin sections (Figure 4) and whole mounts
350 (Figure 5) of the new strains provided details of their internal and external morphological
351 features. The single chloroplast was cup-shaped with a pyrenoid surrounded by starch tubules

352 running through the pyrenoid. The stigma was composed of a single layer of oil droplets
353 (approximately 0.1 μm in diameter) (Figure 4A) and located at the periphery of the chloroplast
354 facing the cell membrane, conforming to the description of the family Mamiellaceae (Marin and
355 Melkonian 2010). Several large ejectosomes composed of fibrils were present at the cell
356 periphery (Figure 4D and E). They are common in the Mamiellales (Moestrup 1984, Marchant et
357 al. 1989) and are perhaps used to deter grazers.
358 One of the most salient features of the Mamiellophyceae is the presence of organic scales
359 covering the cell, the most common of which comprise radiating and concentric ribs resembling
360 spiderwebs that are present in the scale-bearing Mamiellales (*Bathycoccus*, *Mamiella* and
361 *Mantoniella*), as well as *Dolichomastix* (Supplementary Table 3). We examined the whole
362 mounts of the new *Mantoniella* species to establish the presence of scales and determine if they
363 were morphologically distinguishable from related species, as *M. antarctica* (Marchant et al.
364 1989) and *M. gilva* (Moestrup 1984) each have a unique type that differentiate them from other
365 Mamiellales.
366 The flagella and cell bodies of the new strains were covered in imbricated spiderweb-like
367 scales (Figure 5) measuring approximately 0.2 μm. The scales were produced in the Golgi body
368 (Figure 4B). The body scales were sub-quadrangular to oval whereas the flagellar scales were
369 oval (Figure 5). Spiderweb scales had 6–8 major spokes radiating from the center with the
370 number of spokes increasing towards the periphery and six or more concentric ribs dividing the
371 scale into segments. In addition, there were some small scales (approximately 0.1 μm) on the cell
372 body composed of four spokes (increasing to eight) and separated by four, more or less
373 concentric, ribs (Figure 5D, G). The flagella were also covered by lateral hair scales, which were
374 composed of two parallel rows of globular subunits. At the tip of the long flagellum there was a

375 tuft of three hair scales, for which the subunits were more closely packed together than the lateral
376 hair scales (Figure 5). The hair scales of the new strains were identical to the "*Tetraselmis*-type"
377 T-hairs previously described in *Mantoniella* and *Mamiella* (Marin and Melkonian 1994). This
378 structure is otherwise only seen in *Dolichomastix lepidota* and differs from the smooth tubular T-
379 hairs of *Dolichomastix tenuilepis* and *Crustomastix* (Marin and Melkonian 1994, Zingone et al.
380 2002)(Supplementary Table 3).
381 Comparison of the spiderweb scales between *Mantoniella* species (Table 3) showed the new
382 species differ significantly from *M. antarctica*, which possesses lace-like scales with six or seven
383 radial ribs with very few concentric ribs (Marchant et al. 1989). Morphologically, the spiderweb
384 scales of the new species most resembled *M. squamata*, which has large heptaradial flagellar
385 scales, octaradial body scales and a few additional small tetraradial body scales (Marchant et al.
386 1989). Indeed, the spiderweb scales of *M. baffinensis* (Figure 5) were structurally
387 indistinguishable from *M. squamata*. In contrast, *M. beaufortii* shared the small tetraradial body
388 scales but possessed hexaradial flagellar scales and heptaradial body scales, potentially allowing
389 it to be differentiated from the other *Mantoniella* based on the number of radial spokes of the
390 spiderweb scales.
391
392 *Pigment composition.* Pigment to chlorophyll *a* ratios of *M. beaufortii* RCC2288 were compared
393 to a selection of other Chlorophyta species (Figure 6, Supplementary Table 4) from previous
394 studies (Latasa et al. 2004, Lopes dos Santos et al. 2016), as pigments are useful phenotypic
395 traits. Chlorophyll *a* and *b*, characteristics of Chlorophyta, were detected, as well as the basic set
396 of carotenoids found in the prasinophytes: neoxanthin, violaxanthin, lutein, zeaxanthin,
397 antheraxanthin and β-carotene. The additional presence of prasinoxanthin, micromonal and

uriolide placed RCC2288 in the PRASINO-3B group of prasinophyte green algae, *sensu* Jeffrey et al. (2011). This pigment-based grouping showed good agreement with the molecular phylogeny of Mamiellales, where the presence of prasinoxanthin, micromonal and the Unidentified M1 pigment are diagnostic of the order (Marin and Melkonian 2010). We did not detect Unidentified M1 in RCC2288, but as our analysis method differed from previous work (Latasa et al. 2004) and we relied on matching its chromatographic and spectral characteristics, its absence requires further confirmation. Notwithstanding, the pigment complement of RCC2288 was identical to other described Mamiellales (Figure 6, Supplementary Table 4), coherent with its classification within this order.

As noted by Latasa et al. (2004), Mamiellales pigment profiles are remarkably comparable (Figure 6), despite strains being cultured under very different conditions. Only a few carotenoids differed substantially (at least two fold) in relative abundance between *M. beaufortii* and the two other *M. squamata* strains analyzed: the concentration of neoxanthin, antheraxanthin and lutein were higher, whereas that of Mg-DVP and uriolide were relatively lower (Figure 6, Supplementary Table 4). Neoxanthin (associated with the light harvesting complex), as well as antheraxanthin and lutein (both involved in photoprotection), have previously been shown to increase significantly in *M. squamata* grown under continuous light compared to alternating light/dark cycles (Böhme et al. 2002). Therefore, the relatively high ratio of these carotenoids measured in *M. beaufortii* is consistent with growth under continuous light used with RCC2288. Uriolide and Mg-DVP have been observed to increase with light intensity in *M. squamata* (Böhme et al. 2002) and *Micromonas pusilla* (Laviale and Neveux 2011), respectively. Although more physiological data are required to interpret their relative decrease in RCC2288, these pigments are probably most responsive to light conditions (intensity and photoperiod).

Two unknown carotenoids were detected in RC2288, the first one having adsorption peaks at 412, 436 and 464 nm, and the second one at 452 nm (Supplementary Table 5). These were relatively minor components comprising 2.7% and 1.5% of total carotenoids, respectively and may represent carotenoids unique to *M. beaufortii*.

Environmental distribution. In order to obtain information on the distribution of these two new species, we searched by BLAST both environmental GenBank sequences and published 18S V4 and V9 metabarcode data sets (Supplementary Table 2). This allowed the retrieval of a few 18S rRNA sequences with higher than 98% similarity to the gene of RCC2288. Alignment of these sequences with other Mamiellophyceae sequences revealed diagnostic positions in both the V4 and V9 hypervariable regions permitting *M. beaufortii* and *M. baffinensis* to be distinguished from other Mamiellophyceae, especially other *Mamiella* and *Mantoniella* species (Supplementary Figures 1 and 2). Signatures from the V4 region were clearer than from V9 due to the fact that for some of the strains, the sequences did not extend to the end of the V9 region (Supplementary Figure 2). In the V4 region, three signatures were observed, one common to both species (A in Supplementary Figure 1), while the other two (B and C in Supplementary Figure 1) differed between *M. beaufortii* and *baffinensis.*

No clone library or metabarcode sequences matched exactly *M. baffinensis*. In contrast, three environmental sequences (KT814860, FN690725, JF698785) from clone libraries had signatures similar to the *M. beaufortii* strains, two from Arctic Ocean water (Figure 7), including one obtained during the MALINA cruise, and one from ice originating from the Gulf of Finland. V4 metabarcodes corresponding to *M. beaufortii* were found in the Ocean Sampling Day data set (Kopf et al. 2015) that includes more than 150 coastal samples at a single station off East

Greenland as well as in three metabarcoding studies in the Arctic Ocean, one in the Beaufort Sea performed during the MALINA cruise (Monier et al. 2015), one from Arctic sea ice (Stecher et al. 2016) where it was found at three stations and one from the White Sea (Belevich et al. 2017), also in the sea ice (Figure 7). No metabarcode corresponding to these two new species were found in waters from either the Southern Ocean or off Antarctica (Figure 7 and Supplementary Table 2). No metabarcodes from the V9 region corresponding to the two new species were found in the Tara Oceans data set that covered mostly temperate and subtropical oceanic regions (de Vargas et al. 2015). These data suggest that these species are restricted to polar Arctic regions (although we cannot exclude that they may be found in the future in the Antarctic which has been under-sampled until now) and are probably associated to sea ice although they can be present in the sea water, and that *M. beaufortii* is more wide spread than *M. baffinensis*.

Funding

Financial support for this work was provided by the following projects: ANR PhytoPol (ANR-15-CE02-0007) and Green Edge (ANR-14-CE01-0017-03), ArcPhyt (Région Bretagne), TaxMArc (Research Council of Norway, 268286/E40).

Acknowledgments

We thank Adam Monier, Katja Metfies, Estelle Kilias and Wei Luo for communicating raw metabarcoding data and Sophie Le Panse and Antje Hofgaard for assistance with electron microscopy. We acknowledge the support of the BioPIC flow cytometry and microscopy

463 platform of the Oceanological Observatory of Banyuls and of the ABIMS bioinformatics
464 platform at the Roscoff Biological Station.
465

References

Balzano, S., Gourvil, P., Siano, R., Chanoine, M., Marie, D., Lessard, S., Sarno, D. & Vaulot, D. 2012. Diversity of cultured photosynthetic flagellates in the North East Pacific and Arctic Oceans in summer. *Biogeosciences* 9:4553–71.

Balzano, S., Percopo, I., Siano, R., Gourvil, P., Chanoine, M., Marie, D., Vaulot, D. & Sarno, D. 2017. Morphological and genetic diversity of Beaufort Sea diatoms with high contributions from the *Chaetoceros neogracilis* species complex. *J. Phycol.* 53:161–87.

Barlow, S. B. & Cattolico, R. A. 1980. Fine structure of the scale-covered green flagellate *Mantoniella squamata* (Manton et Parke) Desikachary. *Brit. Phycol. J.* 15:321–33.

Belevich, T. A., Ilyash, L. V., Milyutina, I. A., Logacheva, M. D., Goryunov, D. V. & Troitsky, A. V. 2017. Photosynthetic picoeukaryotes in the land-fast ice of the White Sea, Russia. *Microb. Ecol.* 1–16.

Böhme, K., Wilhelm, C. & Goss, R. 2002. Light regulation of carotenoid biosynthesis in the prasinophycean alga *Mantoniella squamata*. *Photochem. Photobiol. Sci.* 1:619–28.

Caisová, L., Marin, B. & Melkonian, M. 2011. A close-up view on ITS2 evolution and speciation - a case study in the Ulvophyceae (Chlorophyta, Viridiplantae). *BMC Evol. Biol.* 11:262.

Coleman, A. W. 2000. The significance of a coincidence between evolutionary landmarks found in mating affinity and a DNA sequence. *Protist* 151:1–9.

Coleman, A. W. 2003. ITS2 is a double-edged tool for eukaryote evolutionary comparisons. *Trends Genet.* 19:370–5.

Coleman, A. W. 2007. Pan-eukaryote ITS2 homologies revealed by RNA secondary structure. *Nucleic Acids Res.* 35:3322–9.

489 de Vargas, C., Audic, S., Henry, N., Decelle, J., Mahe, F., Logares, R., Lara, E., Berney, C., Le
490 Bescot, N., Probert, I., Carmichael, M., Poulain, J., Romac, S., Colin, S., Aury, J.-M.,
491 Bittner, L., Chaffron, S., Dunthorn, M., Engelen, S., Flegontova, O., Guidi, L., Horák, A.,
492 Jaillon, O., Lima-Mendez, G., Lukeš, J., Malviya, S., Morard, R., Mulot, M., Scalco, E.,
493 Siano, R., Vincent, F., Zingone, A., Dimier, C., Picheral, M., Searson, S., Kandels-Lewis,
494 S., *Tara* Oceans Coordinators, Acinas, S. G., Bork, P., Bowler, C., Gorsky, G., Grimsley,
495 N., Hingamp, P., Iudione, D., Not, F., Ogata, H., Pesant, S., Raes, J., Sieracki, M. E.,
496 Speich, S., Stemmann, L., Sunagawa, S., Weissenbach, J., Wincker, P. & Karsenti, E. 2015.
497 Eukaryotic plankton diversity in the sunlit ocean. *Science* 348:1261605.
498 Demir-Hilton, E., Sudek, S., Cuvelier, M. L., Gentemann, C. L., Zehr, J. P. & Worden, A. Z.
499 2011. Global distribution patterns of distinct clades of the photosynthetic picoeukaryote
500 *Ostreococcus*. *ISME J.* 5:1095–107.
501 Derelle, E., Ferraz, C., Escande, M.-L., Eychenié, S., Cooke, R., Piganeau, G., Desdevises, Y.
502 Bellec L., Moreau, H. & Grimsley, N. 2008. Life-cycle and genome of OtV5, a Large DNA
503 virus of the pelagic marine unicellular green alga *Ostreococcus tauri*. *PLoS One*. 3:e2250.
504 Foulon, E., Not, F., Jalabert, F., Cariou, T., Massana, R. & Simon, N. 2008. Ecological niche
505 partitioning in the picoplanktonic green alga *Micromonas pusilla*: Evidence from
506 environmental surveys using phylogenetic probes. *Environ. Microbiol.* 10:2433–43.
507 Guillou, L., Eikrem, W., Chrétiennot-Dinet, M.-J., Le Gall, F., Massana, R., Romari, K., Pedrós-
508 Alió, C. & Vaulot, D. 2004. Diversity of picoplanktonic prasinophytes assessed by direct
509 nuclear SSU rDNA sequencing of environmental samples and novel isolates retrieved from
510 oceanic and coastal marine ecosystems. *Protist* 155:193–214.
511 Guindon, S., Dufayard, J.-F., Lefort, V. & Anisimova, M. 2010. New algorithms and methods to

estimate maximum-likelihoods phylogenies: Assessing the performance of PhyML 3.0. *Syst. Biol.* 59:307–21.

Hu, Y. O. O., Karlson, B., Charvet, S. & Andersson, A. F. 2016. Diversity of pico- to mesoplankton along the 2000 km salinity gradient of the baltic sea. *Front. Microbiol.* 7:1–17.

Jeffrey, S. W., Wright, S. W. & Zapata, M. 2011. Microalgal classes and their signature pigments. *In* Roy, S., Llewellyn, C. A., Egeland, E. S. & Johnsen, G. [Eds.] *Phytoplankton Pigments: Characterization, Chemotaxonomy and Applications in Oceanography.* Cambridge Univ Press, Cambridge. 3–77 pp.

Katoh, K. & Toh, H. 2008. Recent developments in the MAFFT multiple sequence alignment program. *Brief. Bioinform.* 9:286–98.

Kearse, M., Moir, R., Wilson, A., Stones-Havas, S., Cheung, M., Sturrock, S., Buxton, S., Cooper, A., Markowitz, S., Duran, C., Thierer, T., Ashton, B., Meintjes, P. & Drummond, A. 2012. Geneious Basic: An integrated and extendable desktop software platform for the organization and analysis of sequence data. *Bioinformatics* 28:1647–9.

Keller, M. D., Selvin, R. C., Claus, W. & Guillard, R. R. L. 1987. Media for the culture of oceanic ultraphytoplankton. *J. Phycol.* 23:633–8.

Kopf, A., Bicak, M., Kottmann, R., Schnetzer, J., Kostadinov, I., Lehmann, K., Fernandez-Guerra, A., Jeanthon, C., Rahav, E., Ullrich, M., Wichels, A., Gunnar, G., Polymenakou, P., Kotoulas, G., Siam, R., Abdallah, R. Z., Sonnenschein, E. C., Cariou, T., O'Gara, F., Jackson, S., Orlic, S., Steinke, M., Busch, J., Duarte, B., Caçador, I., Canning-Clode, J., Bobrova, O., Marteinsson, V., Reynisson, E., Loureiro, C. M., Luna, G. M., Quero, G. M., Löscher, C. R., Kremp, A., DeLorenzo, M. E., Øvreås, L., Tolman, J., LaRoche, J., Penna,

A., Frischer, M., Davis, T., Katherine, B., Meyer, C. P., Ramos, S., Magalhães, C., Jude-Lemeilleur, F., Aguirre-Macedo, M. L., Wang, S., Poulton, N., Jones, S., Collin, R., Fuhrman, J. A., Conan, P., Alonso, C., Stambler, N., Goodwin, K., Yakimov, M. M., Baltar, F., Bodrossy, L., Van De Kamp, J., Frampton, D. M. F., Ostrowski, M., Van Ruth, P., Malthouse, P., Claus, S., Deneudt, K., Mortelmans, J., Pitois, S., Wallom, D., Salter, I., Costa, R., Schroeder, D. C., Kandil, M. M., Amaral, V., Biancalana, F., Santana, R., Pedrotti, M. L., Yoshida, T., Ogata, H., Ingleton, T., Munnik, K., Rodriguez-Ezpeleta, N., Berteaux-Lecellier, V., Wecker, P., Cancio, I., Vaulot, D., Bienhold, C., Ghazal, H., Chaouni, B., Essayeh, S., Ettamimi, S., Zaid, E. H., Boukhatem, N., Bouali, A., Chahboune, R., Barrijal, S., Timinouni, M., El Otmani, F., Bennani, M., Mea, M., Todorova, N., Karamfilov, V., ten Hoopen, P., Cochrane, G., L'Haridon, S., Bizsel, K. C, Vezzi, A., Lauro, F. M., Martin, P., Jensen, R. M., Hinks, J., Gebbels, S., Rosselli, R., De Pascale, F., Schiavon, R., dos Santos, A., Villar, E., Pesant, S., Cataletto, B., Malfatti, F., Edirisinghe, R., Herrera Silveira, J. A., Barbier, M., Turk, V., Tinta, T., Fuller, W. J., Salihoglu, I., Serakinci, N., Ergoren, M. C., Bresnan, E., Iriberri, J., Nyhus, P. A. F., Bente, E., Karlsen, H. E., Golyshin, P. N., Gasol, J. M., Moncheva, S., Dzhembekova, N., Johnson, Z., Sinigalliano, C. D., Gidley, M. L., Zingone, A., Danovaro, R., Tsiamis, G., Clark, M. S., Costa, A. C., El Bour, M., Martins, A. M., Collins, R. E., Ducluzeau, A.-L., Martinez, J., Costello, M. J.m Amaral-Zettler, L. A., Gilbert, J. A., Davies, N., Field, D. & Glöckner, O. 2015. The ocean sampling day consortium. *Gigascience* 4:27.

Latasa, M., Scharek, R., Le Gall, F. & Guillou, L. 2004. Pigment suites and taxonomic groups in Prasinophyceae. *J. Phycol.* 40:1149–55.

Laviale, M. & Neveux, J. 2011. Relationships between pigment ratios and growth irradiance in

11 marine phytoplankton species. *Mar. Ecol. Prog. Ser.* 425:63–77.

Lopes dos Santos, A., Gourvil, P., Rodríguez, F., Garrido, J. L. & Vaulot, D. 2016. Photosynthetic pigments of oceanic Chlorophyta belonging to Prasinophytes clade VII. *J. Phycol.* 52:148–55.

Lopes dos Santos, A., Gourvil, P., Tragin, M., Noël, M. H., Decelle, J., Romac, S. & Vaulot, D. 2017a. Diversity and oceanic distribution of prasinophytes clade VII, the dominant group of green algae in oceanic waters. *ISME J.* 11:512–28.

Lopes dos Santos, A., Pollina, T., Gourvil, P., Corre, E., Marie, D., Garrido, J. L., Rodríguez, F., Noël, M.-H., Vaulot, D. & Eikrem, W. 2017b. Chloropicophyceae, a new class of picophytoplanktonic prasinophytes. *Sci. Rep.* 7:14019.

Lovejoy, C., Vincent, W. F., Bonilla, S., Roy, S., Martineau, M. J., Terrado, R., Potvin, M., Massana, R. & Pedrós-Alió, C. 2007. Distribution, phylogeny, and growth of cold-adapted picoprasinophytes in Arctic seas. *J. Phycol.* 43:78–89.

Mai, J. C. & Coleman, A. W. 1997. The internal transcribed spacer 2 exhibits a common secondary structure in green algae and flowering plants. *J. Mol. Evol.* 44:258–71.

Manton, I. & Parke, M. 1960. Further observations on small green flagellates with special reference to possible relatives of *Chromulina pusilla* Butcher. *J. Mar. Biol. Assoc.* 39:275–98.

Marchant, H. J., Buck, K. R., Garrison, D. L. & Thomsen, H. A. 1989. *Mantoniella* in Antarctic waters including the description of *M. antarctica* sp. nov. (Prasinophyceae). *J. Phycol.* 25:167–74.

Marin, B. & Melkonian, M. 1994. Flagellar hairs in prasinophytes (Chlorophyta): Ultrastructure and distribution on the flagellar surface. *J. Phycol.* 30:659–78.

581 Marin, B. & Melkonian, M. 2010. Molecular phylogeny and classification of the
582 Mamiellophyceae class. nov. (Chlorophyta) based on sequence comparisons of the nuclear-
583 and plastid-encoded rRNA operons. *Protist* 161:304–36.
584 Massjuk, N.P. 2006. Chlorodendrophyceae class. nov. (Chlorophyta, Viridiplantae) in the
585 Ukrainian flora: I. Phylogenetic relations and taxonomical status. *Ukr. Bot. J.* 63:601–14.
586 Moestrup, Ø. 1984. Further studies on *Nephroselmis* and its allies (Prasinophyceae). II. *Mamiella*
587 gen. nov., Mamiellaceae fam. nov., Mamiellales ord. nov. *Nord. J. Bot.* 4:109–21.
588 Moestrup, Ø. & Throndsen, J. 1988. Light and electron microscopical studies on
589 *Pseudoscourfieldia marina*, a primitive scaly green flagellate (Prasinophyceae) with
590 posterior flagella. *Can. J. Bot.* 66:1415–34.
591 Monier, A., Me Comte, J., Babin, M., Forest, A., Matsuoka, A. & Lovejoy, C. 2015.
592 Oceanographic structure drives the assembly processes of microbial eukaryotic
593 communities. *ISME J.* 9:990–1002.
594 Müller, T., Philippi, N., Dandekar, T., Schultz, J. & Wolf, M. 2007. Distinguishing species. *RNA*
595 13: 1469–72.
596 Not, F., Massana, R., Latasa, M., Marie, D., Colson, C., Eikrem, W., Pedrós-Alió, C., Vaulot, D.
597 & Simon, N. 2005. Late summer community composition and abundance of photosynthetic
598 picoeukaryotes in Norwegian and Barents Seas. *Limnol. Oceanogr.* 50:1677–86.
599 Palenik, B., Grimwood, J., Aerts, A., Rouzé, P., Salamov, A., Putnam, N., Dupont, C.,
600 Jorgensen, R., Derelle, E., Rombauts, S., Zhou, K., Otillar, R., Merchant, S. S., Podel, S.,
601 Gaasterland, T., Napoli, C., Gendler, K., Manuell, A., Tai, V., Vallon, O., Piganeau, G.,
602 Jancek, S., Heijde, M., Jabbari, K., Bowler, C., Lohr, M., Robbens, S., Werner, G.,
603 Dubchak, I., Pazour, G. J., Ren, Q., Paulsen, I., Delwiche, C., Schmutz, J., Rokhsar, D., Van

de Peer, Y., Moreau, H. & Grigoriev, I. V. 2007. The tiny eukaryote *Ostreococcus* provides genomic insights into the paradox of plankton speciation. *P. Natl. Acad. Sci. U.S.A.* 104:7705–10.

Park, M. & Rayns, D. G. 1964. Studies on marine flagellates. VII. *Nephroselmis gilva* sp. nov. and some allied forms. *J. Mar. Biol. Ass. U.K.* 44:209–17.

Piganeau, G., Eyre-Walker, A., Grimsley, N. & Moreau, H. 2011. How and why DNA barcodes underestimate the diversity of microbial eukaryotes. *PLoS One*. 6:e16342.

Ras, J., Claustre, H. & Uitz, J. 2008. Spatial variability of phytoplankton pigment distributions in the Subtropical South Pacific Ocean: comparison between *in situ* and predicted data. *Biogeosciences* 5:353–69.

Rodríguez, F., Derelle, E., Guillou, L., Le Gall, F., Vaulot, D. & Moreau, H. 2005. Ecotype diversity in the marine picoeukaryote *Ostreococcus* (Chlorophyta, Prasinophyceae). *Environ. Microbiol.* 7:853–9.

Ronquist, F. & Huelsenbeck, J. P. 2003. MrBAYES 3: Bayesian phylogenetic inference under mixed models. *Bioinformatics* 19:1572–4.

Schultz, J., Maisel, S., Gerlach, D., Müller, T. & Wolf, M. 2005. A common core of secondary structure of the internal transcribed spacer 2 (ITS2) throughout the Eukaryota. *RNA* 11:361–4.

Seibel, P., Müller, T., Dandekar, T. & Wolf, M. 2008. Synchronous visual analysis and editing of RNA sequence and secondary structure alignments using 4SALE. *BMC Res. Notes*. 1:91.

Sherr, E.B., Sherr, B.F., Wheeler, P. A. & Thompson, K. 2003. Temporal and spatial variation in stocks of autotrophic and heterotrophic microbes in the upper water column of the central Arctic Ocean. *Deep Sea Research Part I: Oceanographic Research Papers* 50:557–71.

627 Simmons, M. P., Sudek, S., Monier, A., Limardo, A. J., Jimenez, V., Perle, C. R., Elrod, V. A.,
628 Pennington, J. T. & Worden, A. Z. 2016. Abundance and biogeography of picoprasinophyte
629 ecotypes and other phytoplankton in the eastern North Pacific Ocean. *Appl. Environ.*
630 *Microbiol.* 82:1693–705.
631 Simon, N., Foulon, E., Grulois, D., Six, C., Desdevises, Y., Latimier, M., Le Gall, F., Tragin, M.,
632 Houdan, A., Derelle, E., Jouenne, F., Marie, D., Le Panse, S., Vaulot, D. & Marin, B. 2017.
633 Revision of the genus *Micromonas* Manton et Parke (Chlorophyta, Mamiellophyceae), of
634 the type species *M. pusilla* (Butcher) Manton et Parke of the species *M. commoda* van
635 Baren, Bachy and Worden and description of two new species based on the genetic and
636 phenotypic characterization of cultured isolates. *Protist* 168:612–35.
637 Subirana, L., Péquin, B., Michely, S., Escande, M-L., Meilland, J., Derelle, E., Marin, B.,
638 Piganeau, G., Desdevises, Y., Moreau, H. & Grimsley, N. H. 2013. Morphology, genome
639 plasticity, and phylogeny in the genus *Ostreococcus* reveal a cryptic species,
640 *O. mediterraneus* sp. nov. (Mamiellales, Mamiellophyceae). *Protist* 164: 643–659.
641 Stecher, A., Neuhaus, S., Lange, B., Frickenhaus, S., Beszteri, B., Kroth, P.G. & Valentin, K.
642 2016. rRNA and rDNA based assessment of sea ice protist biodiversity from the central
643 Arctic Ocean. *Eur. J. Phycol.* 51:31–46.
644 Tamura, K., Stecher, G., Peterson, D., Filipski, A. & Kumar, S. 2013. MEGA6: Molecular
645 evolutionary genetics analysis version 6.0. *Mol. Biol. Evol.* 30:2725–9.
646 Thiers, B. Index Herbariorum: A global directory of public herbaria and associated staff. New
647 York Botanical Garden's Virtual Herbarium. Available at: http://sweetgum.nybg.org/ih (last
648 accessed 20 August 2019)
649 Throndsen, J. & Kristiansen, S. 1991. *Micromonas pusilla* (Prasinophyceae) as part of pico- and

650 nanoplankton communities of the Barents Sea. *Polar Res.* 10:201–7.
651 Tragin, M., Lopes dos Santos, A., Christen, R. & Vaulot, D. 2016. Diversity and ecology of
652 green microalgae in marine systems: An overview based on 18S rRNA gene sequences.
653 *Perspect. Phycol.* 3:141–54.
654 Tragin, M. & Vaulot, D. 2018. Green microalgae in marine coastal waters: The Ocean Sampling
655 Day (OSD) dataset. *Sci. Rep.* 8:1–12.
656 Treusch, A. H., Demir-Hilton, E., Vergin, K. L., Worden, A. Z., Carlson, C. A, Donatz, M. G.,
657 Burton, R. M. & Giovannoni, S. J. 2012. Phytoplankton distribution patterns in the
658 northwestern Sargasso Sea revealed by small subunit rRNA genes from plastids. *ISME J.*
659 6:481–92.
660 Turmel, M., Lopes dos Santos, A., Otis, C., Sergerie, R. & Lemieux, C. 2019. Tracing the
661 evolution of the plastome and mitogenome in the Chloropicophyceae uncovered convergent
662 tRNA gene losses and a variant plastid genetic code. *Genome Biol. Evol.* 11: 1275–92.
663 Zingone, A., Borra, M., Brunet, C., Forlani, G., Kooistra, W. H. C. F. & Procaccini, G. 2002.
664 Phylogenetic position of *Crustomastix stigmatica* sp. nov. and *Dolichomastix tenuilepsis* in
665 relation to the Mamiellales (Prasinophyceae, Chlorophyta). *J. Phycol.* 38:1024–39.
666 Zuker, M. 2003. Mfold web server for nucleic acid folding and hybridization prediction. *Nucleic*
667 *Acids Res.* 31:3406–15.
668
669
670
671
672

673 *Figures*

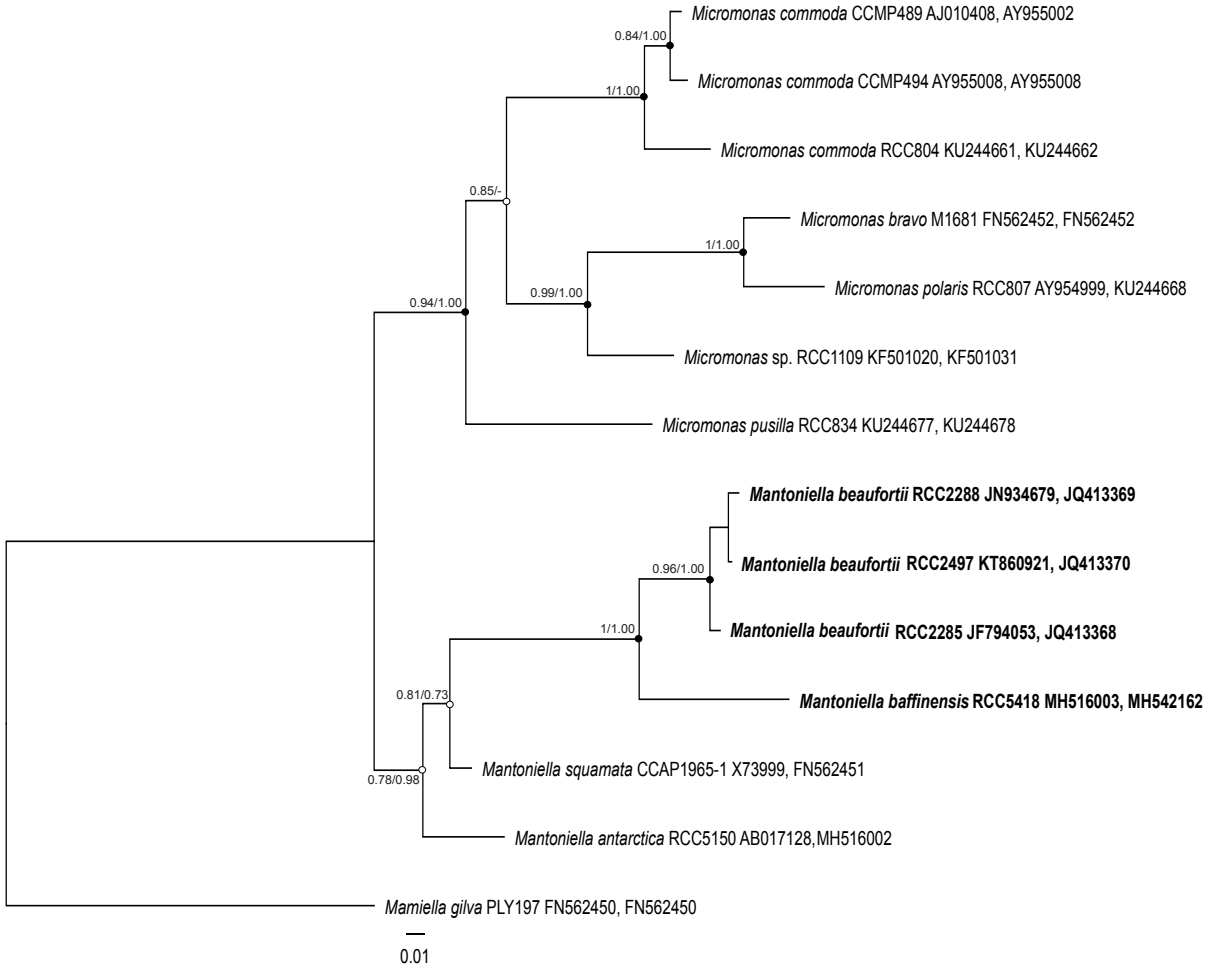

674

675 Figure 1. Maximum-likelihood tree inferred from concatenated 18S/ITS2 sequences of
676 Mamiellaceae. Solid dots correspond to nodes with significant support (> 0.8) for ML analysis
677 and Bayesian analysis (> 0.95). Empty dots correspond to nodes with non-significant support for
678 either ML or Bayesian analysis, or both.

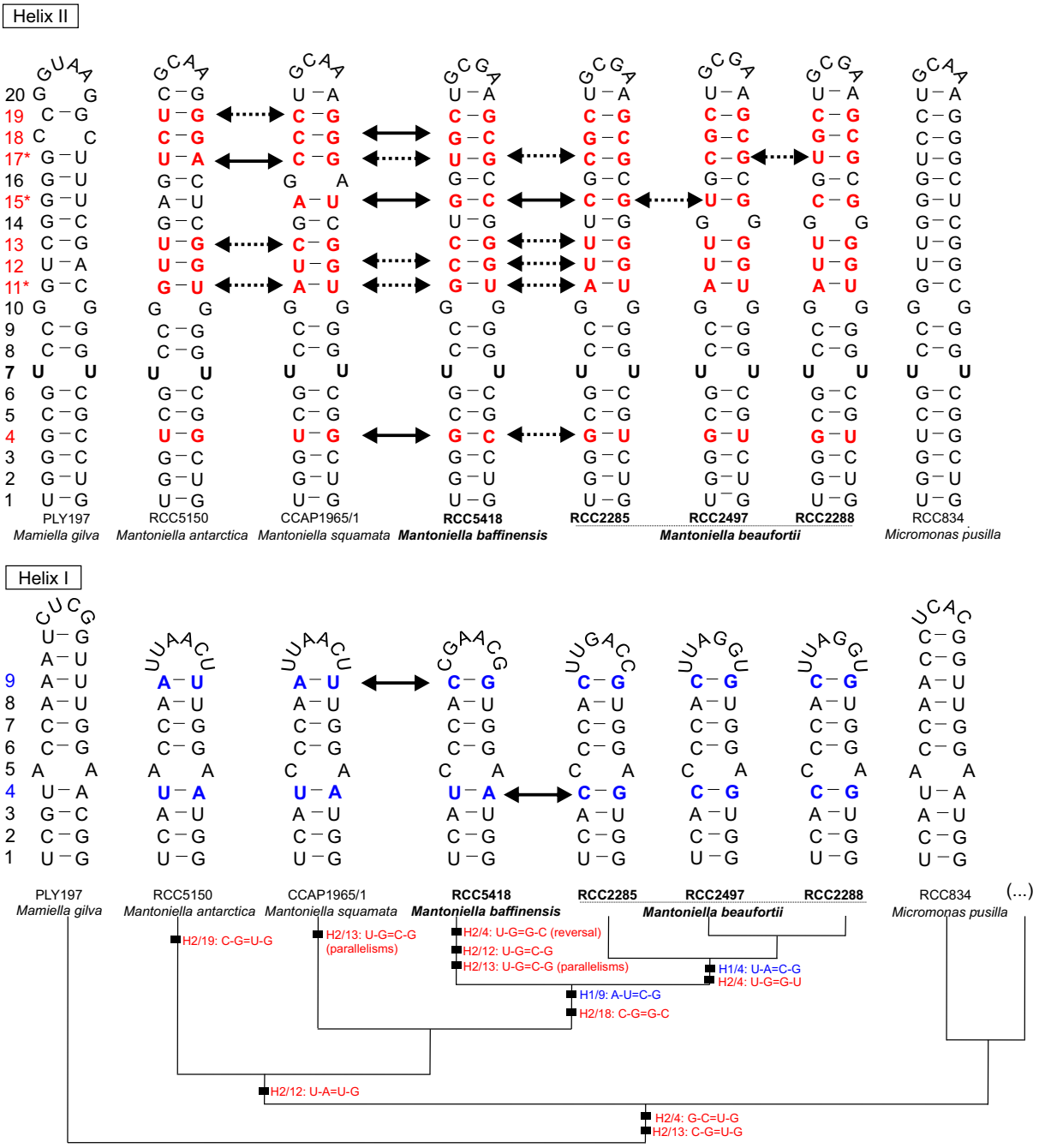

679

680 Figure 2. Molecular signatures of *Mantoniella* species based on comparison of ITS2 secondary
681 structures within Mamiellaceae. Signatures in Helix I are shown in blue and Helix II in red. The
682 conserved base pairs among the different groups are numbered. Compensatory base changes
683 (CBCs) and hemi-CBCs (hCBSs) are highlighted by solid and dotted arrows respectively.

Hypervariable positions are marked by an asterisk (*). Ellipsis (…) represent the other clades and species of *Micromonas*. The pyrimidine-pyrimidine (Y-Y) mismatch in Helix II is shown in bold black. Single nucleotide substitutions are shown by grey nucleotides. Identified homoplasious changes are shown as parallelisms and reversals.

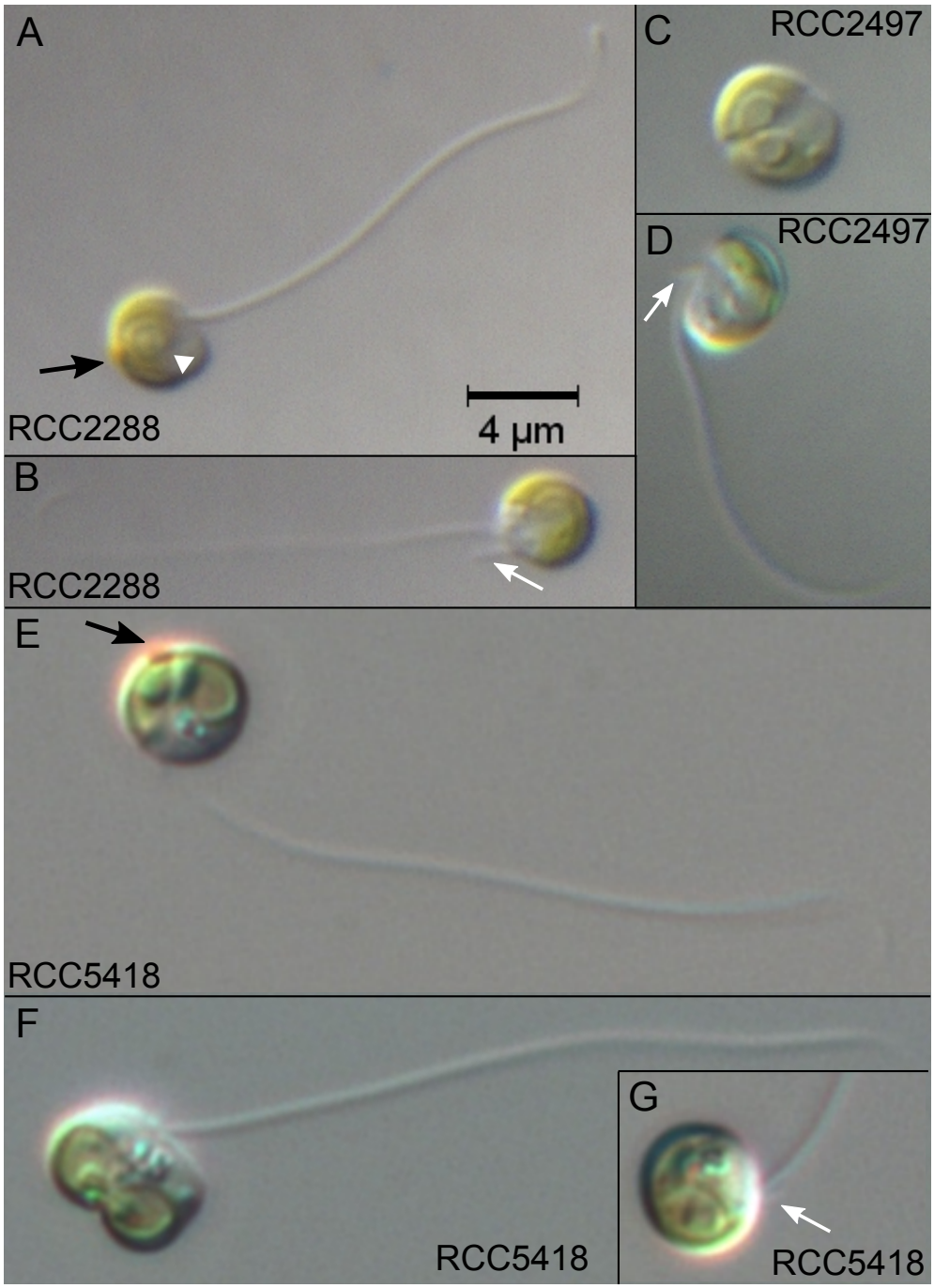

Figure 3. Light microscopy images of the new *Mantoniella* strains. All strains have round cell morphology, visible red stigma (black arrow), a long and short flagellum (white arrow) and one chloroplast with a pyrenoid (white arrowhead). Scale bar is 4 μm for all images. (**A**–**B**) *M. beaufortii* RCC2288. (**C**–**D**) *M. beaufortii* RCC2497 during cell division and single cell showing long and short flagellum. (**E**–**G**) *M. baffinensis* RCC5418 single cell (**E**), during cell division (**F**) and cell showing the short flagellum (**G** inset).

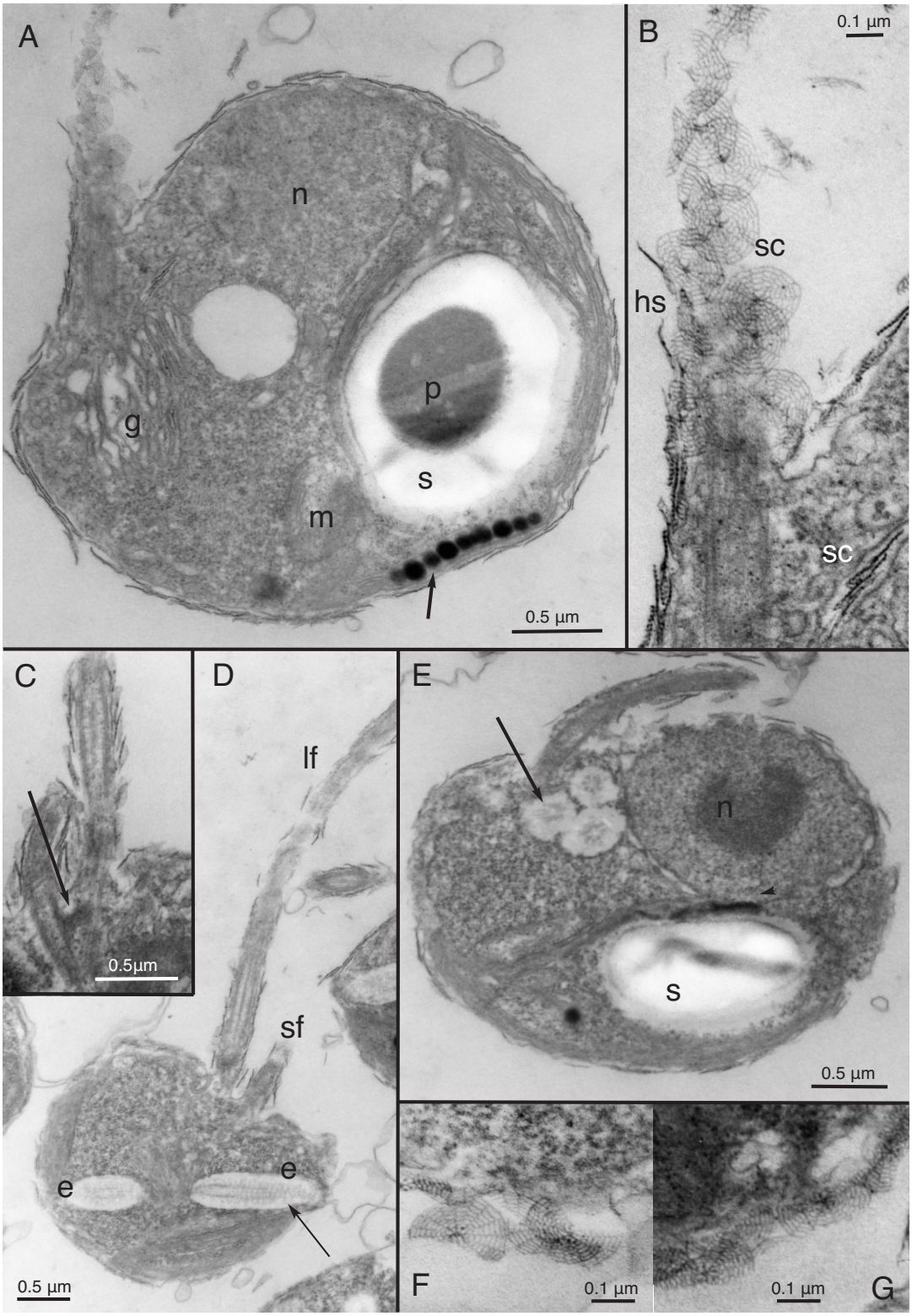
A
n
p
g
s
m
0.5 µm
B
0.1 µm
sc
hs
sc
C
0.5µm
D
lf
sf
e
e
0.5 µm
E
n
s
0.5 µm
F
0.1 µm
0.1 µm
G

695

Figure 4. TEM thin sections of *M. beaufortii* RCC2288. (**A**) Internal cell structure showing organelles and stigma (black arrow). (**B**) Detail of the hair and spiderweb scales covering the long flagellum. Scales produced in the Golgi body. (**C**) Detail of the flagellar base (black arrow). (**D**) Cell with long and short flagella and longitudinal section of the ejectosomes (black arrow). (**E**) Cross section of ejectosomes (black arrow). (**F**) and (**G**) body scales made up of radiating and concentric ribs. Abbreviations: e=ejectosome, g=Golgi, s=starch granule, m=mitochondrion, n=nucleus, p=pyrenoid, hs=hair scale, sc=scale, lf=long flagellum and sf=short flagellum.

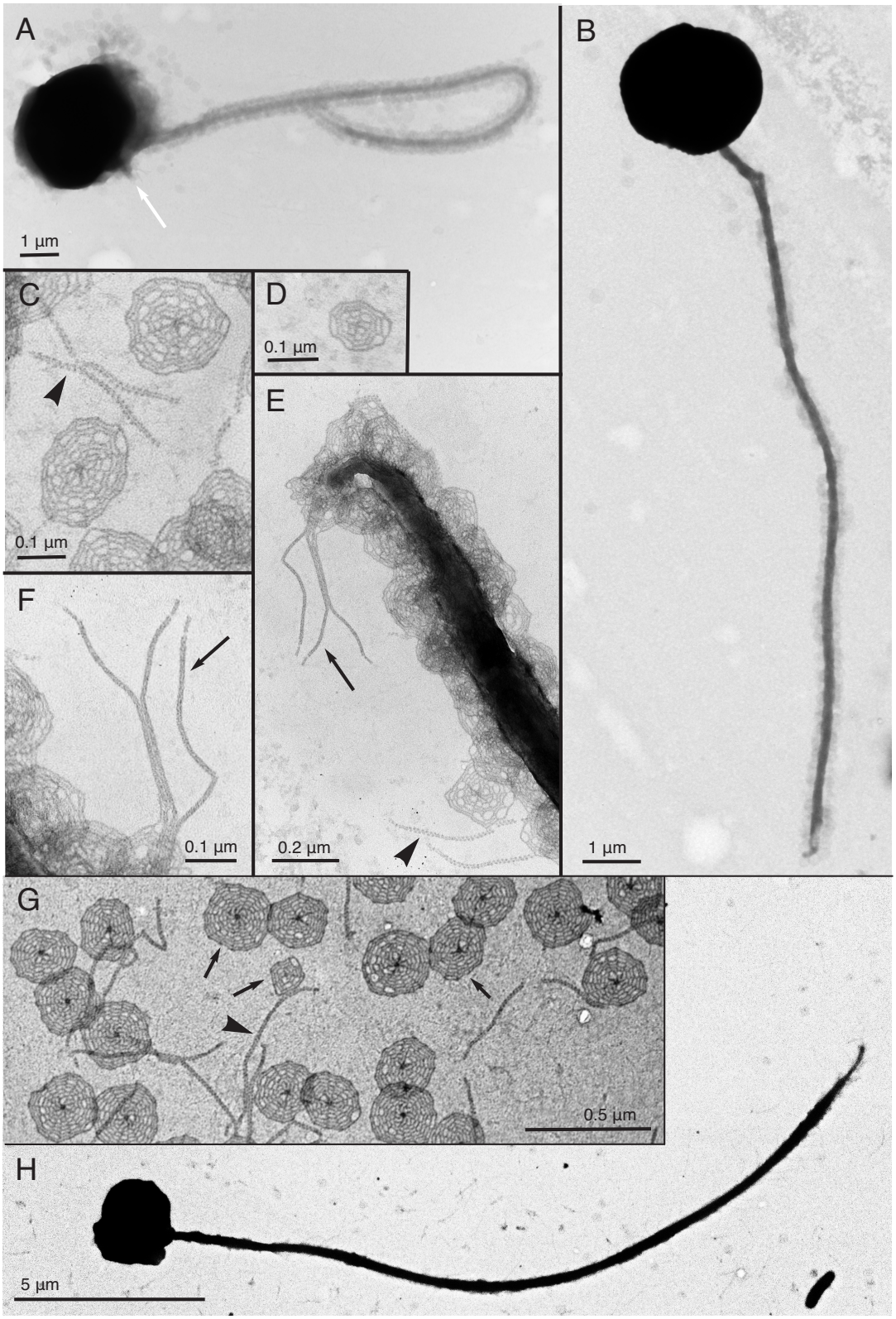

703

Figure 5. Transmission electron micrographs of whole-mounts of the new *Mantoniella* strains. (**A**–**E**) *M. beaufortii.* (**A**) Whole cells of strain RCC2288, indicating the short flagellum (white arrow), and (**B**) RCC2497. (**C**) Detached flagellar spiderweb-like scales and hair scales (black arrowhead). (**D**) Detail of small tetraradial body scale. (**E**) Imbricated scales and hair scales covering the long flagellum. A tuft of three hair scales on the tip of the long flagellum (black arrow) (**F**) Detail of the tuft of hair scales (black arrow). (**G**–**H**) *M. baffinensis* RCC5418. (**G**) Small and large body scales (black arrows) and flagellar hair scales (black arrowhead) and (**H**) whole cell.

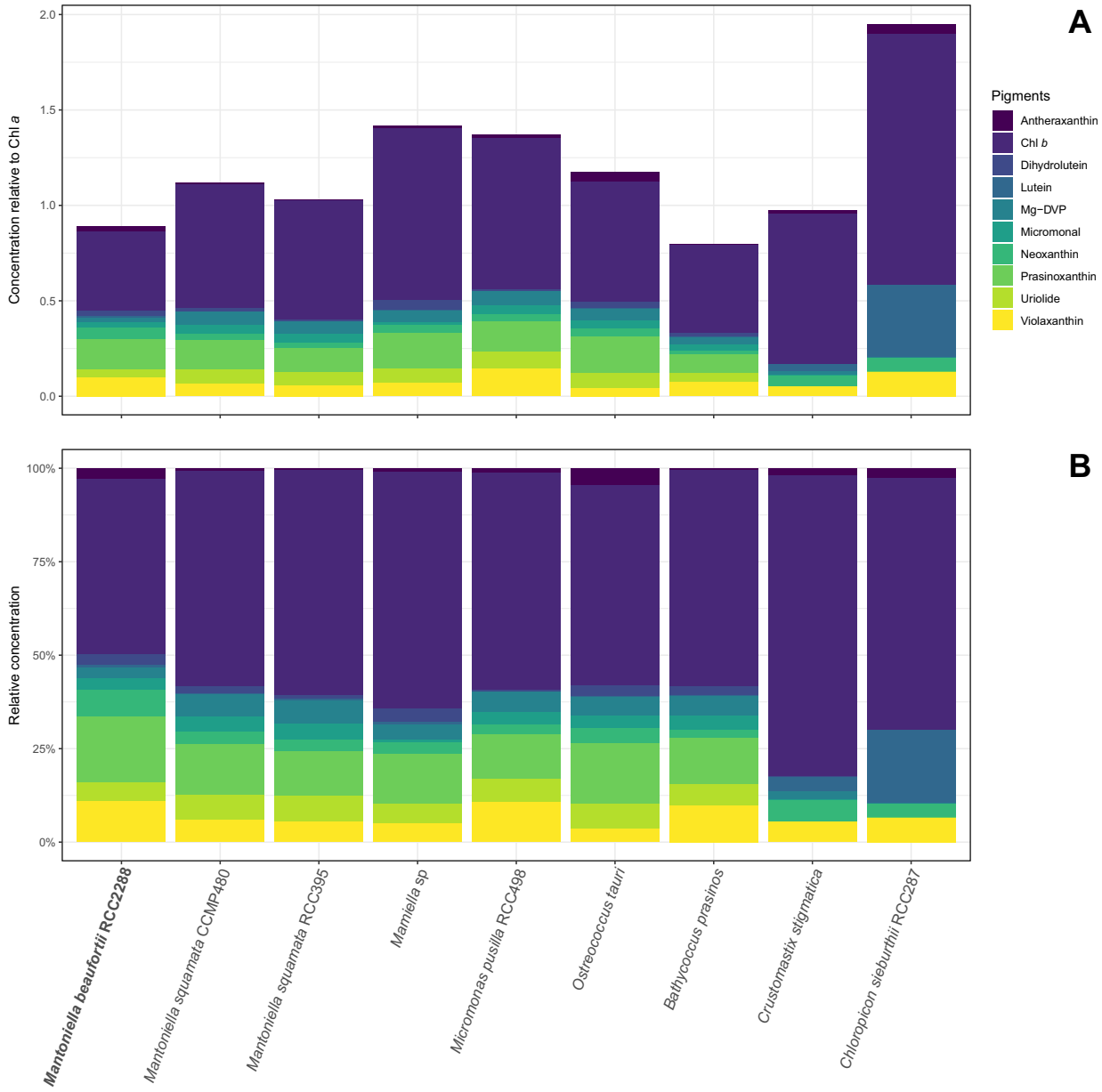

Figure 6. Pigment to chlorophyll *a* ratios in *M. beaufortii* RCC2288 (this study) compared to other Mamiellophyceae species (data from Latasa et al. 2004). (**A**) Cumulative pigment to Chlorophyll *a* ratio of Chlorophyll *b* and abundant carotenoids (excluding α- and β-carotene). (**B**) As for **A**, but showing relative abundances. Mg-DVP: Mg-24-divinyl pheoporphyrin *a*5 monomethyl ester.

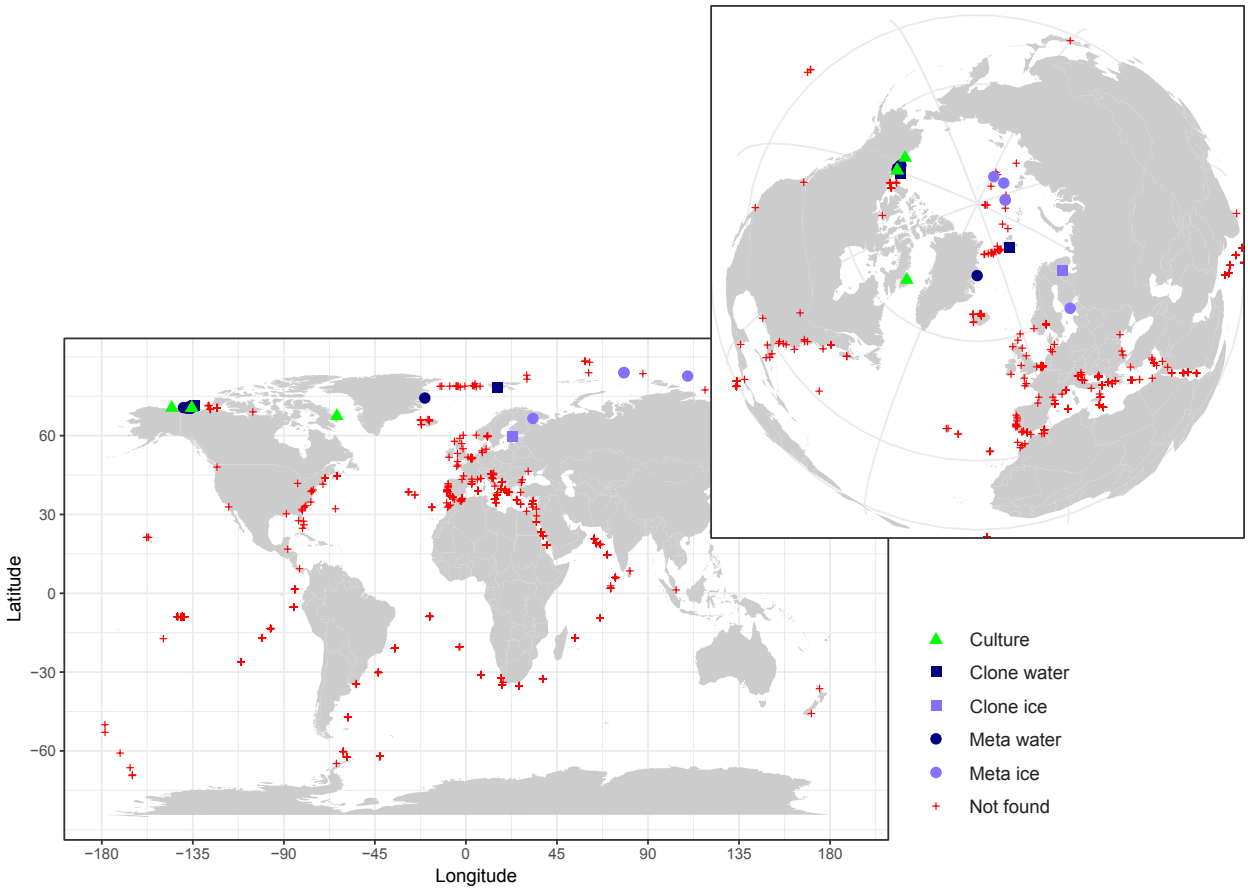

Figure 7. Map of the distribution of *M. beaufortii* in environmental sequence datasets highlighting its prevalence in Arctic samples (inset). The isolation sites of *M. beaufortii* cultures, presence of its 18S rRNA gene sequence in clone libraries (Clone water, Clone ice) and metabarcodes from seawater and ice samples (Meta water, Meta ice) and absence in metabarcodes (Not found) are plotted. For *M. baffinensis*, only its isolation site is indicated in Baffin Bay since no similar environmental sequence was found in the datasets analyzed. Metabarcoding datasets include Ocean Sampling Day, Tara Oceans and polar projects. See Supplementary Table 2 for a full description of the metabarcoding datasets screened.

Tables

Table 1. Strains used in this study. RCC: Roscoff Culture Collection (www.roscoff-culture-collection.org). 18S rRNA and ITS show Genbank accession numbers. Strains in bold used to describe the new species.

Strain	Strain Name	Oceanic Region	Latitude	Longitude	Depth of Isolation (m)	18S rRNA	ITS	Remark
RCC2285	MALINA E43.N1	Beaufort Sea	70° 34' N	145° 24' W	0	JF794053	JQ413368	strain lost
RCC2288	MALINA E47.P2	Beaufort Sea	70° 30' N	135° 30' W	0	JN934679	JQ413369	
RCC2497	MALINA E47.P1	Beaufort Sea	70° 30' N	135° 30' W	0	KT860921	JQ413370	
RCC5418	GE_IP_IC_DIL_490	Baffin Bay	67° 28' N	63° 46' W	surface ice	MH516003	MH542162	

Table 2. Cell diameter and long flagellum lengths measured for *M. beaufortii* (RCC2288 and RCC2497) and *M. baffinensis* (RCC5418). n = number of cells measured and SD = standard deviation.

Strain	min	max	mean	median	stdev	n
	Cell diameter (µm)					
RCC2288	2.89	4.98	3.77	3.70	0.41	60
RCC2497	3.15	4.74	3.87	3.77	0.39	39
RCC5418	3.54	5.69	4.66	4.66	0.51	69
	Long flagellum length (µm)					
RCC2288	12.93	21.47	16.27	15.99	2.63	11
RCC2497	11.91	21.25	16.31	17.07	2.71	12
RCC5418	11.27	32.59	21.78	21.29	5.14	25

Table 3. Comparison of *Mantoniella* spp. scale types.

Species	Flagellar scales	Body scales
Mantoniella squamata	spiderweb-like heptaradial	spiderweb-like large octoaradial and small rare tetraradial
Mantoniella antarctica	lace-like heptaradial	lace-like hexaradial and smaller heptaradial
Mantoniella beaufortii	spiderweb-like hexaradial	spiderweb-like large heptaradial and small rare tetraradial
Mantoniella baffinensis	spiderweb-like heptaradial	spiderweb-like large octoaradial and small rare tetraradial

Supplementary Figures

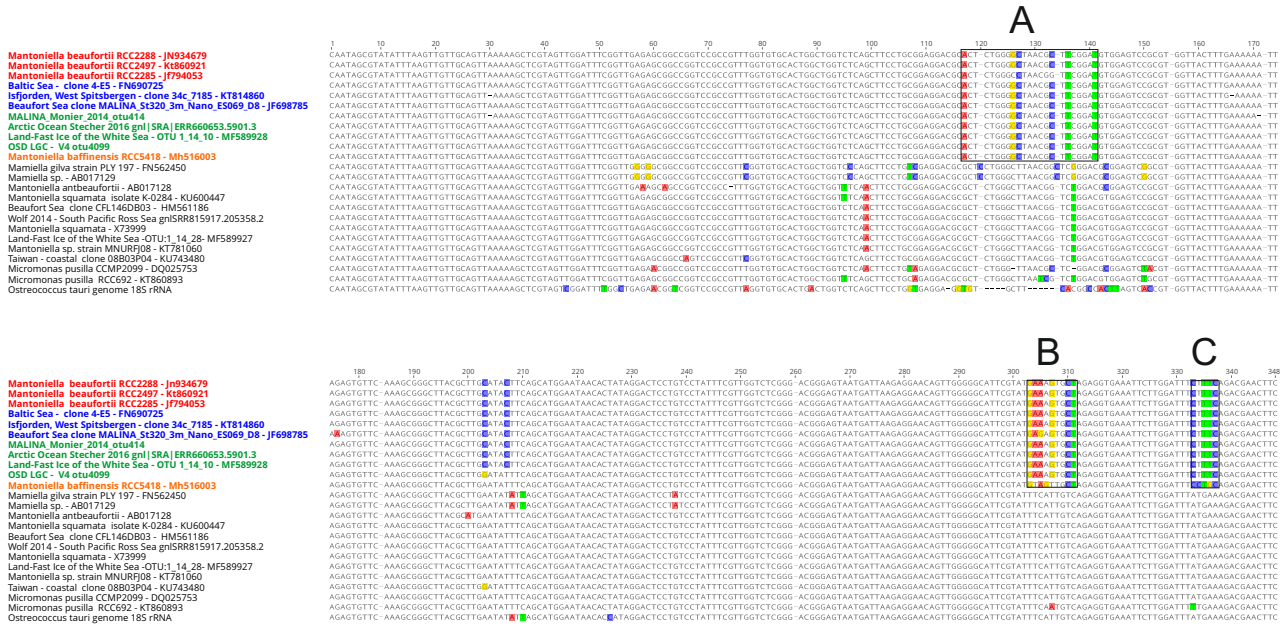

Supplementary Figure 1. Alignment of the 18S rRNA gene V4 hypervariable region from *M. beaufortii* and *M. baffinensis* strains (Red and Orange, respectively), environmental clones (Blue) and metabarcodes (Green) with a selection of sequences from closely related Mamiellophyceae. Sequence signatures diagnostic of the two new species are indicated by boxes. The A region is specific of both species while the B and C regions differ between the two species.

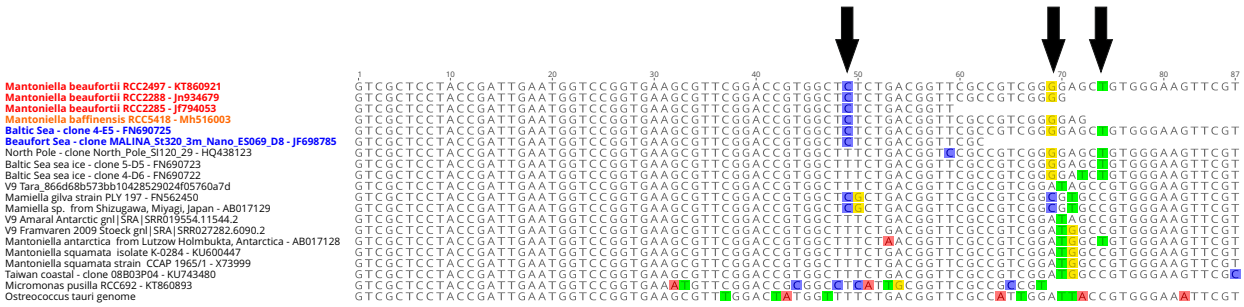

Supplementary Figure 2. Alignment of the 18S rRNA gene V9 hypervariable region from *M. beaufortii* and *M. baffinensis* strains (Red and Orange, respectively) and environmental clones (blue) with a selection of closely related Mamiellophyceae sequences. Sequence signatures diagnostic of *M. beaufortii* and *M. baffinensis* are indicated by arrows.

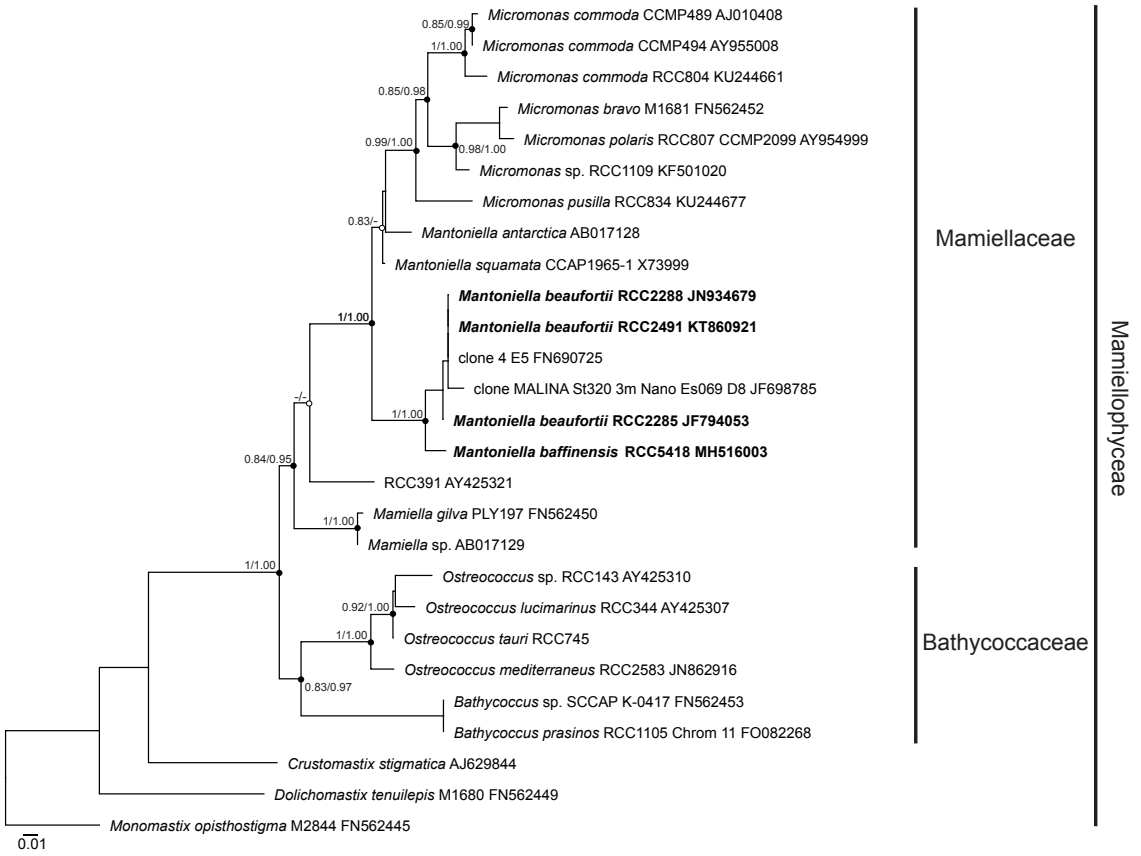

761

762 Supplementary Figure 3. Maximum-likelihood phylogenetic tree inferred from nuclear 18S
763 rRNA sequences of Mamiellophyceae. *Monomastix opisthostigma* was used as an outgroup.
764 Solid dots correspond to nodes with significant support (> 0.8) for ML analysis and Bayesian
765 analysis (>0.95). Empty dots correspond to nodes with non-significant support for either ML or
766 Bayesian analysis, or both. GenBank accessions of the 18S rRNA sequences shown after the
767 species name.

768

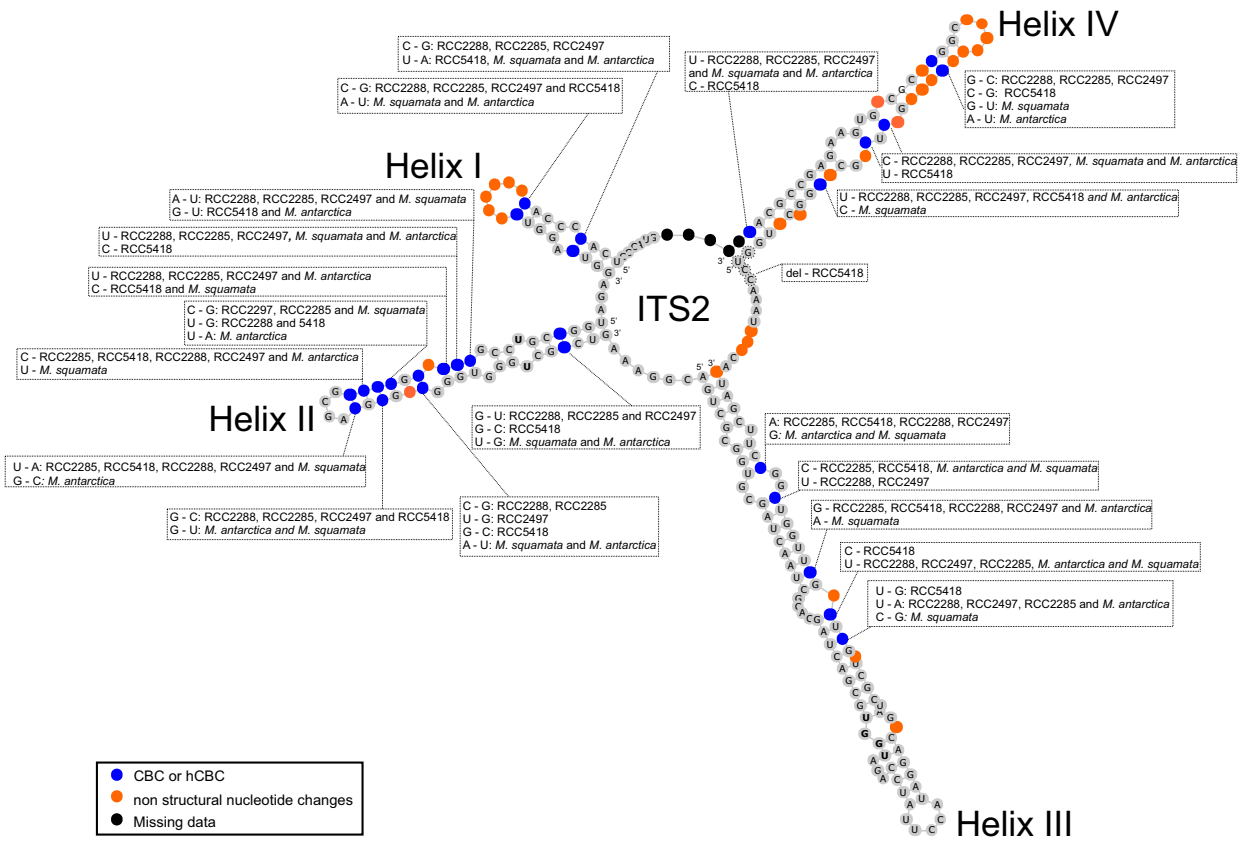

769

770 Supplementary Figure 4. Intramolecular folding pattern of the ITS2 molecule of *Mantoniella*

771 (RCC2288, RCC2285, RCC2497 and RCC5418). The four major helices are labeled as Helix I –

772 Helix IV. Blue dots represent either CBCs or hCBCs. Non-CBCs (N – N ↔ N × N) are

773 represented in orange.

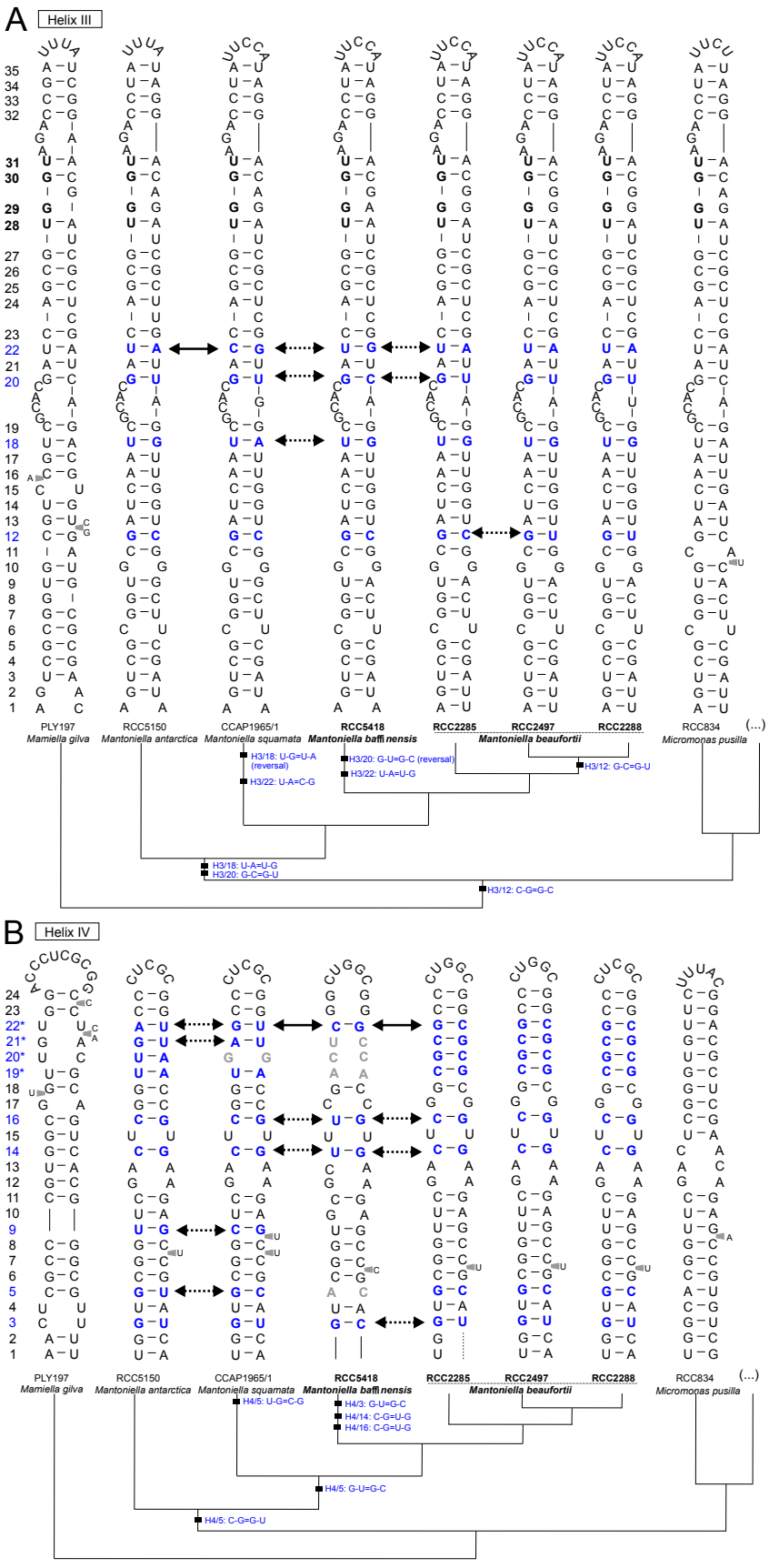
A
Helix III
PLY197
Mamiella gilva
RCC5150
Mantoniella antarctica
CCAP1965/1
Mantoniella squamata
RCC5418
Mantoniella baffinensis
RCC2285
RCC2497
RCC2288
Mantoniella beaufortii
RCC834
Micromonas pusilla
(...)
H3/18: U-G=U-A (reversal)
H3/22: U-A=C-G
H3/20: G-U=G-C (reversal)
H3/22: U-A=U-G
H3/12: G-C=G-U
H3/18: U-A=U-G
H3/20: G-C=G-U
H3/12: C-G=G-C
B
Helix IV
PLY197
Mamiella gilva
RCC5150
Mantoniella antarctica
CCAP1965/1
Mantoniella squamata
RCC5418
Mantoniella baffinensis
RCC2285
RCC2497
RCC2288
Mantoniella beaufortii
RCC834
Micromonas pusilla
(...)
H4/5: U-G=C-G
H4/3: G-U=G-C
H4/14: C-G=U-G
H4/16: C-G=U-G
H4/5: G-U=G-C
H4/5: C-G=G-U

774

Supplementary Figure 5. Molecular signatures of *Mantoniella* species revealed by comparison of ITS2 secondary structures within Mamiellaceae. Signatures in Helix III are shown in (**A**) and Helix IV in (**B**). The conserved base pairs among the different groups are numbered. CBCs and hCBCs are highlighted by solid and dotted arrows, respectively. Hypervariable positions are marked by an asterisk (*). Ellipsis (…) represent the other clades and species of *Micromonas*. The YRRY (pyrimidine-purine-pyrimidine) motif on the 5' side arm of Helix III is shown in bold black. Single nucleotide substitutions are shown by grey nucleotides. Identified homoplasious changes are shown as parallelisms and reversals.

Supplementary Tables

Supplementary Table 1. Primers and PCR conditions used in this study. Abbreviations: fwd - forward, rev. - reverse, temp - temperature.

Gene	Primer fwd	Sequence 5'-3'	Primer rev.	Sequence 5'-3'	Reference	cycles	Initial time	Denaturation temp	Denaturation time	Annealing temp	Annealing time	Annealing temp	Extension time	Extension temp	Elongation time	Elongation temp
18S rRNA	Euk63F	ACGCTTGTCTCAAAGATTA	Euk1818R	ACGGAAACCTTGTTACGA	Lepère et al. 2011	35	5 min	95ºC	30 sec	95ºC	30 sec	55ºC	1 min 30 sec	72ºC	10 min	72ºC
ITS1-5.8S-ITS2	329f	GTGAACCTGCRGAAGGATCA	D1R-R	TATGCTTAAATTCAGCGGGT	Balzano et al. 2017	35	5 min	95ºC	1 min	95ºC	45 sec	55ºC	1 min 15 sec	72ºC	7 min	72ºC

Supplementary Table 2. Metabarcoding datasets of the 18S rRNA gene analyzed in this study for the presence of *M. beaufortii* and *M. baffinensis* signatures.

Data set	18S region	Region	Samples	Bioproject or link	Sequencer	Clustering	Reference
Tara Oceans	V9	Oceanic	334	http://doi.pangaea.de/10.1594/PANGAEA.843022	Illumina	Swarm	de Vargas, C., Audic, S., Henry, N., Decelle, J., Mahe, F., Logares, R., et al. (2015). Eukaryotic plankton diversity in the sunlit ocean. Science 348, 1261605. doi:10.1126/science.1261605.
OSD - LGC - 2014	V4	Coastal	157	PRJEB8682	Illumina	0.97	Kopf, A., Bicak, M., Kottmann, R., Schnetzer, J., Kostadinov, I., Lehmann, K., Fernandez-Guerra, A. et al. 2015. The ocean sampling day consortium. Gigascience. 4:27.
MALINA - Monier - 2014	V4	Arctic Ocean	24	PRJNA202104	454	0.98	Monier, A., Terrado, R., Thaler, M., Comeau, A., Medrinal, E. & Lovejoy, C. 2013. Upper Arctic Ocean water masses harbor distinct communities of heterotrophic flagellates. Biogeosciences. 10:4273–86. Monier, A., Comte, J., Babin, M., Forest, A., Matsuoka, A. & Lovejoy, C. 2014. Oceanographic structure drives the assembly processes of microbial eukaryotic communities. ISME J. 9:990–1002.
ACME - Comeau - 2011	V4	Arctic Ocean	11	SRA029114	454	0.98	Comeau, A. M., Li, W. K. W., Tremblay, J.-É., Carmack, E. C. & Lovejoy, C. Arctic Ocean microbial community structure before and after the 2007 record sea ice minimum. PLoS One 6, e27492 (2011)
Nansen Basin - Metfies - 2016	V4	Arctic Ocean	17	PRJEB11449	454	0.97	Metfies, K., von Appen, W.-J., Kilias, E., Nicolaus, A. & Nöthig, E.-M. Biogeography and Photosynthetic Biomass of Arctic Marine Pico-Eukaroytes during Summer of the Record Sea Ice Minimum 2012. PLoS One 11, 20 pp. (2016)
Southern Ocean - Wolf - 2014	V4	Southern Ocean	6	PRJNA176875	454	0.97	Wolf, C., Frickenhaus, S., Kilias, E. S., Peeken, I. & Metfies, K. Protist community composition in the Pacific sector of the Southern Ocean during austral summer 2010. Polar Biol. 37, 375–389 (2014)
Fieldes Bay - Luo - 2016	V4	Southern Ocean	10	PRJNA254097	Illumina	0.97	Luo, W. et al. Molecular diversity of microbial eukaryotes in sea water from Fildes Peninsula, King George Island, Antarctica. Polar Biol. (2015). doi:10.1007/s00300-015-1815-8
Fram Strait - Kilias - 2013	V4	Arctic Ocean	5		454	0.97	Kilias, E., Wolf, C., Nöthig, E.-M., Peeken, I. & Metfies, K. Protist distribution in the Western Fram Strait in summer 2010 based on 454-pyrosequencing of 18S rDNA. J. Phycol. 49, 996–1010 (2013).

802 Supplementary Table 3. Morphological characters in Mamiellophyceae species.

Species	Flagella	Spider web-like scales	Circular patterned scales	T-hair scales: tubular shaft	T-hair scales: globular subunits
Bathycoccus prasinos	no	+	-	-	-
Ostreococcus tauri	no	-	-	-	-
Ostreoccoccus mediterraneus	no	-	-	-	-
Mamiella gilva	2 long	+	-	-	+
Mantoniella squamata	1 long, 1 short	+	-	-	+
Mantoniella antarctica	1 long, 1 short	+	-	-	+
Mantoniella beaufortii	1 long, 1 short	+	-	-	+
Mantoniella baffinensis	1 long, 1 short	+	-	-	+
Micromonas pusilla	1 long, 2 extending microtubules	-	-	-	-
Micromonas commoda	1 long, 2 extending microtubules	-	-	-	-
Micromonas polaris	1 long, 2 extending microtubules	-	-	-	-
Micromonas bravo	1 long, 2 extending microtubules	-	-	-	-
Crustomastix didyma	2 long	-	-	+	-
Crustomastix stigmatica	2 long	-	-	+	-
Dolichomastix eurylepidea	2 long	+	-	?	?
Dolichomastix lepidota	2 long	-	-	-	+
Dolichomastix nummulifera	2 long	-	+	?	?
Dolichomastix tenuilepsis	2 long	+	+	+	-

803

804

805

806

807

808

809

810

Supplementary Table 4. Pigment composition of *M. beaufortii* (RCC2288) compared to a selection of green algae. Values are shown as a ratio of pigment to Chl *a* concentration and percent contribution to total carotenoids (in italics). See Supplementary Table 5 for the full names of the pigments.

Species	Order	Phytn a	Chld a	Chl b	Mg-DVP	%	Uri	%	Neo	%	Pra	%	Vio	%	Mmnal	%	Ant	%	Lut	%	Dihy	%	α-car + β-car	%
***M. beaufortii* RCC2288**	Mamiellales	0.006	0.012	0.416	0.024	*3.6*	0.045	*6.6*	0.063	*9.4*	0.156	*23.2*	0.099	*14.6*	0.028	*4.2*	0.025	*3.7*	0.006	*0.9*	0.027	*4.0*	0.167	*24.8*
M. squamata CCMP480*	Mamiellales	ND	ND	0.644	0.068	*10.1*	0.075	*11.1*	0.04	*5.5*	0.15	*22.2*	0.068	*10.1*	0.045	*6.7*	0.006	*0.9*	0.003	*0.4*	0.021	*3.1*	0.121	*17.9*
M. squamata RCC395*	Mamiellales	ND	ND	0.62	0.065	*12.2*	0.073	*13.7*	0.03	*5.8*	0.123	*23.1*	0.056	*10.5*	0.043	*8.1*	0.003	*0.6*	0.004	*0.8*	0.009	*1.7*	0.062	*11.7*
O. tauri RCC116*	Mamiellales	ND	ND	0.633	0.061	*8.6*	0.079	*11.1*	0.05	*6.3*	0.191	*26.9*	0.044	*6.2*	0.039	*5.5*	0.051	*7.2*	0.003	*0.4*	0.032	*4.5*	0.098	*13.8*
B. prasinos RCC113*	Mamiellales	ND	ND	0.462	0.041	*9.7*	0.047	*11.1*	0.02	*4.3*	0.097	*22.9*	0.078	*18.4*	0.03	*7.1*	0.002	*0.5*	0.003	*0.7*	0.018	*4.3*	0.029	*6.9*
M. pusilla CCMP490*	Mamiellales	ND	ND	0.768	0.072	*9.7*	0.096	*13.0*	0.05	*6.1*	0.191	*25.8*	0.103	*13.9*	0.053	*7.2*	0.019	*2.6*	0.006	*0.8*	0.01	*1.3*	0.058	*7.8*
Mamiella sp. RCC391*	Mamiellales	ND	ND	0.896	0.060	*8.7*	0.072	*10.5*	0.04	*6.3*	0.189	*27.6*	0.074	*10.8*	0.01	*1.5*	0.011	*1.6*	0.008	*1.2*	0.052	*7.6*	0.082	*12.0*
*C. stigmatica**	Dolichomastigales	ND	ND	0.786	0.023	*3.5*	0	*0*	0.06	*8.4*	0	*0*	0.055	*8.3*	0	*0*	0.017	*2.6*	0.038	*5.7*	0	*0*	0.305	*45.9*
C. sieburthii RCC287†	Chloropicales	ND	0.106	0.986	0	*0*	0	*0*	0.17	*14.8*	0	*0*	0.572	*50.8*	0	*0*	0.024	*2.1*	0.363	*32.2*	0	*0*	-	-
P. parkeae CCMP724*	Pyramimonadales	ND	ND	0.677	0.001	*0.4*	0	*0*	0	*0*	0	*0*	0.077	*27.7*	0	*0*	0.002	*0.7*	0.07	*25.2*	0	*0*	0.088	*31.7*
N. pyriformis CCMP717*	Nephrodelmidaceae	ND	ND	0.698	0.015	*3.5*	0	*0*	0.02	*5.0*	0	*0*	0.077	*18.2*	0	*0*	0.016	*3.8*	0.022	*5.2*	0	*0*	0.065	*15.3*
Tetraselmis sp. RCC234*	Chlorodendrales	ND	ND	0.812	0.022	*4.6*	0	*0*	0.03	*6.8*	0	*0*	0.057	*11.8*	0	*0*	0.006	*1.2*	0.096	*19.9*	0	*0*	0.082	*17.0*
*P. marina**	Pseudoscourfieldiales	ND	ND	0.871	0.071	*13.3*	0	*0*	0.06	*10.7*	0.287	*53.8*	0.036	*6.8*	0	*0*	0	*0*	0.003	*0.6*	0	*0*	0.033	*6.2*
P. capsulatus CCMP1192*	Prasinococcales	ND	ND	0.62	0.098	*16.7*	0.097	*16.6*	0.08	*13.0*	0.183	*31.2*	0.035	*6.0*	0	*0*	0.001	*0.2*	0.015	*2.6*	0.005	*0.9*	0.025	*4.3*

*Values from Latasa et al. 2004, †Values from Lopes dos Santos et al. 2016.

825 Supplementary Table 5. Pigments analyzed in this study. LOD, limit of detection.

Pigment	Abbreviation	Retention time (min)	Detection adsorption wavelength (nm)	LOD (ng/inj)	LOD in 1 L filtered (mg.m-3)
Mg-24-divinyl pheoporphyrin *a*5 monomethyl ester	MgDVP	6.3	450	0.015	0.0004
Chlorophyllide *a* and Chlorophyllide *a*-lik	Chld *a* + Chlo	6.3	667	0.016	0.0004
Uriolide	Uri	11.6	450	ND	ND
Neoxanthin	Neo	13.5	450	0.008	0.0002
Prasinoxanthin	Pra	14.0	450	0.008	0.0002
Violaxanthin	Vio	14.3	450	0.010	0.0002
Micromonal	Mmnal	15.0	450	ND	ND
Antheraxanthin	Ant	16.3	450	0.012	0.0004
Unknown carotenoid λmax 412, 436, 46	Unk 1	16.5	450	ND	ND
Unknown carotenoid λmax 452 nm	Unk 2	18.1	450	ND	ND
Lutein	Lut	18.3	450	0.012	0.0002
Dihydrolutein	Dihy	18.6	450	ND	ND
Chlorophyll *b*-degradation product	Chl*b*-deg	22	450	ND	ND
Chlorophyll *b*	Chl *b*	22.4	450	0.004	0.0001
Chlorophyll *b*-like	Chl *b-like*	22.8	450	0.004	0.0001
Chlorophyll a, allomers and epimers	Chl *a*	24.3	667	0.011	0.0002
Phaeophytin *a* and Phaeophytin *a*-like	Phytn *a* + Ph	25.9	667	0.006	0.0002
α-Carotene and β-Carotene	α-car + β-car	26.9	450	0.012	0.0004

826

827